Chapter 4

Results and Discussion

Chapter 4 enumerates the effect of welding parameters such as current, voltage, gas flow rate and heat input on mechanical and metallurgical properties of GMA Weld joints respectively.

4 Results and Discussion

4.1 Introduction

The effect of heat input on different welding parameters such as current, voltage and gas flow rate on weldability of MIG welded joints of A6061 and A6063 has been thoroughly evaluated through experimentation. The weldability of welded joints would be significantly influenced by welding conditions and can be assessed through the mechanical and microstructural analysis of the welded joints. Hence in this investigation, tensile strength, microstructure and microhardness measurements were carried out on the cross-section of the weldment. Experiments were carried out using Instron Universal testing machine, Vickers microhardness tester, and X-ray radiography, Optical Microscope, Scanning Electron Microscope (SEM), and X-ray Diffraction (XRD). Hence in this chapter, a complete analysis has been carried out to understand the influence of welding parameters on mechanical and metallurgical behaviour of MIG joints of A6061and A6063 aluminium alloy. The details related to the fabrication of joints, specimen preparation, dimensions, and testing procedures for various tests were presented in Chapter 3.

4.2 Heat Input Calculations

Heat input plays an essential role in defining the total heat available for fusion welding and can find the amount of dilution. Higher heat input increases the dilution and penetration level and defects quantity. As the gas flow rate has lower effect on heat input during welding, So HI for samples of medium gas flowrate of 14LPM has been only given.

$$\textbf{Heat Input (HI)} = \mu\frac{V\times I}{S\times 100}\ (\text{kJ/cm})$$

Where, **μ** =Welding efficiency (μ =0.8 used)

HI = Heat Input (kJ/cm)

V =Welding voltage (volts)

I = Welding current (Amp)

S = Travel speed (mm/s)

Other Constant Parameters: **Polarity:** Direct Current Electrode Negative

Filler wire: A4043

Diameter: 1.6 mm

Torch angle: 15degree

Torch to work distance: 15 mm

Table 4.1: Calculation of HI for Various welding parameters

Sample No.	Current (Amp)	Voltage (Volts)	Weld speed (mm/s)	Heat Input (kJ/cm)
1.	140	15	2.5	6.72
2.	140	18	2.5	8.06
3.	140	21	2.5	9.40
4.	160	15	2.5	7.680
5.	160	18	2.5	9.216
6.	160	21	2.5	10.752
7.	180	15	2.5	8.640
8.	180	18	2.5	10.368
9.	180	21	2.5	12.096

A welding efficiency (μ) of 0.8 for GMAW process has been used because thermal efficiency of MIG process is high (0.8), as most of the heat generated is utilized in the melting of electrode and base metal (R.S. Funderburk, 1999).

Electrode-negative (straight polarity) welding results in higher ($2/3^{rd}$) heat concentration on the workpiece side and adequate melting of the electrode, resulting, good weld joints are possible to be made.

L9 has been chosen as it reduces the total number of experiments and overall cost of experimentation.

4.3 Visual Inspection

The joints of A6061and A6063 aluminium alloy were successfully fabricated by MIG welding using the different welding parameters. The fabricated joint has been displayed in Fig. 4.1 and Fig. 4.2. The top surface of the welded joints for optimum parameters are free from visible defects.

4.3.1 Visual Inspection A6061

Welded specimens was cleaned with acetone and observed for various welding defects like lack of fusion, undercuts, spatters and Penetration. Macroscopic features were also examined for both materials. Similar macroscopic features were found for A6061 and A6063 welded joints. High levels of spatter have been found for higher levels of current, voltage and gas flow rate. Elliptical weld bead ripple can be seen clearly for sample welded at Current-160A, Voltage-18V and gas flowrate-14lpm with lowest spatter can be seen from Fig. 4.1 (a-c).

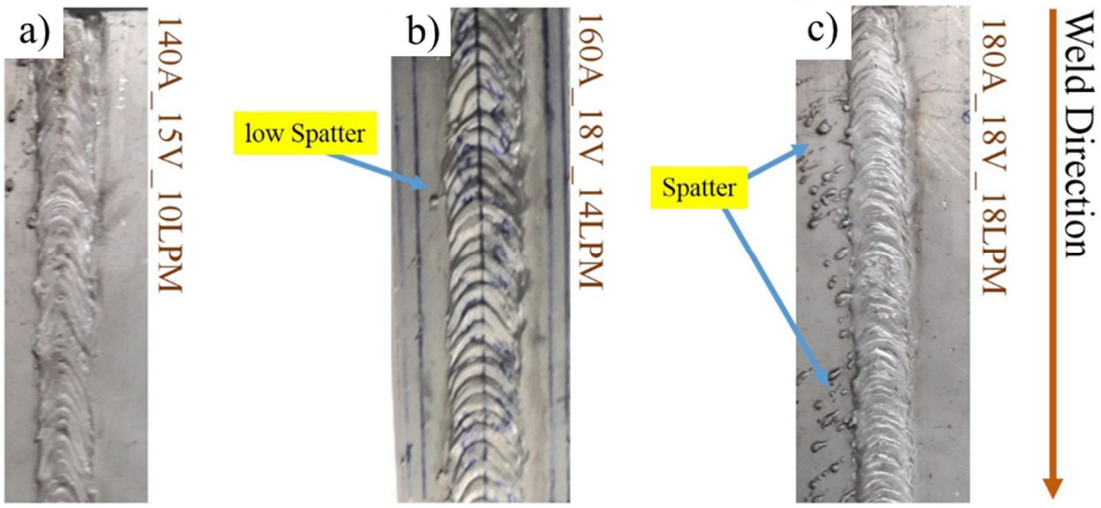

Figure 4.1: a) 140A_15V_18lpm, b) 160A_18V_14lpm, c) 180A_18V_18lpm

A lower level of current and voltage produced narrower bead width as a lower current caused a lower metal deposition rate and changes the shape of weld ripples to trapezoidal

shape. The higher current levels caused excessive spatter and ripples transformed to approximately circular in nature due to increased heat input.

4.3.2 Visual Inspection A6063

Similar results have been found for A6063, like elongated trapezoidal bead ripples on the surface with a slightly higher level of spatters with respect to A6061 as shown in Fig. 4.2 having Minimum Spatter and weld with elliptical weld bead ripples on the top surface for 160A_18V_14lpm parameters. Slightly wider ripples and bead width have been observed.

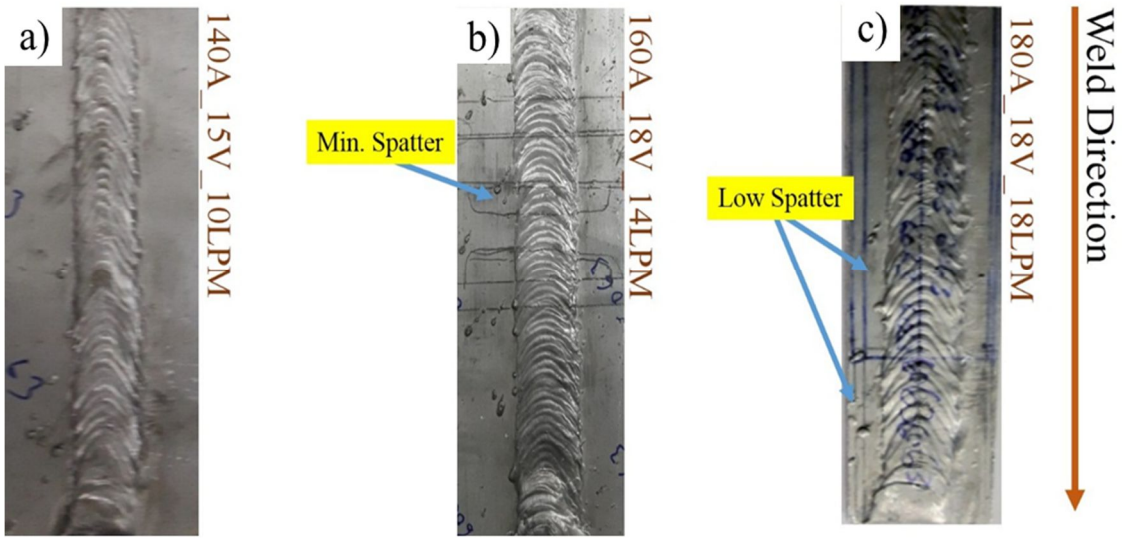

Figure 4.2: a) 140A_15V_10lpm, b) 160A_18V_14lpm, c) 180A_18V_18lpm

4.4 Macrostructure of the MIG Welded Joints

Table 4.1shows macroscopic views of the cross-section indicate the Penetration and gases trapped inside the weld, i.e. porosity or blow holes inside the fusion zone. Blowholes and lower levels of penetration has been observed for joints produced at the current of 140A and gas flow rate of 18lpm for both materials, as shown in Fig. 4.3. An increase in voltage produced a slight increase in the width of the weld bead and similar

observations were found for change of voltage during welding. Welded joints have no defects inside the weld bead except the low Penetration validated by radiography images.

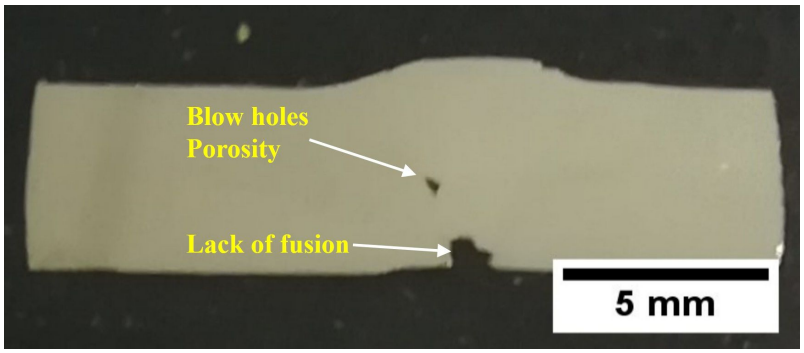

Figure 4.3: Blowholes and lower levels of Penetration for 140A_15V_10lpm

4.4.1 Effect of Welding Parameters on weld bead and Penetration

From the macrographs, it was concluded that there is the complete fusion between the weld and parent metal observed in the joints produced using all types of parameters and also found free from defects. The weld area indicates that the shielding gas configuration has a pronounced effect on the melting efficiency, resulting in a greater weld area on the constant argon base case. The welds were produced using all types of parameters resulted in similar weld bead width. Pure argon produces arc plasma in which the arc energy is more uniformly dispersed. The argon arc plasma is characterized by a very high-energy inner core and an outer mantle of lesser heat energy (Hilton & Norrish et al. 1988. This difference in characteristics of arc strongly affects the weld bead profile. Argon arc produces a bead profile most often characterized by a capillary type penetration pattern.

Table 4.2: Heat Inputs: (a) 6.7kJ/cm, (b) 9.4kJ/cm, (c) 8.6kJ/cm, (d) 12.1kJ/cm

Gas Flow Rate	Heat Input	Macro structure	Penetration
10LPM	(a) 6.7kJ/cm		Full Penetration
14LPM	(b) 9.4kJ/cm		Full Penetration
18LPM	(c) 8.6kJ/cm		Full Penetration

In the present study, gas flow rate 14LPM Heat Inputs: (a) 6.7kJ/cm, (b) 9.4kJ/cm, (c) 8.6kJ/cm, (d) 12.1kJ/cm showed deeper and broader Penetration compared with gas flow rate 10LPM and 18LPM.

4.4.2 Effect of Welding Parameters on Porosity

The application of shielding gases can reduce the level of porosity present within the weld. This is mainly attributed to the dynamic action that the weld pool experiences due to the fluctuation between shielding gas flow rates and environments. For the observation of weld porosity for welded specimens, X-ray radiographic tests for welds were performed and radiographic images are displayed in Fig. 4.3. In the X-ray radiographic test, porosities on X-ray film for all the welded specimens were investigated. In addition to this number of porosity in the weld, the region was determined by analyzing the optical micrograph images of the weld pool.

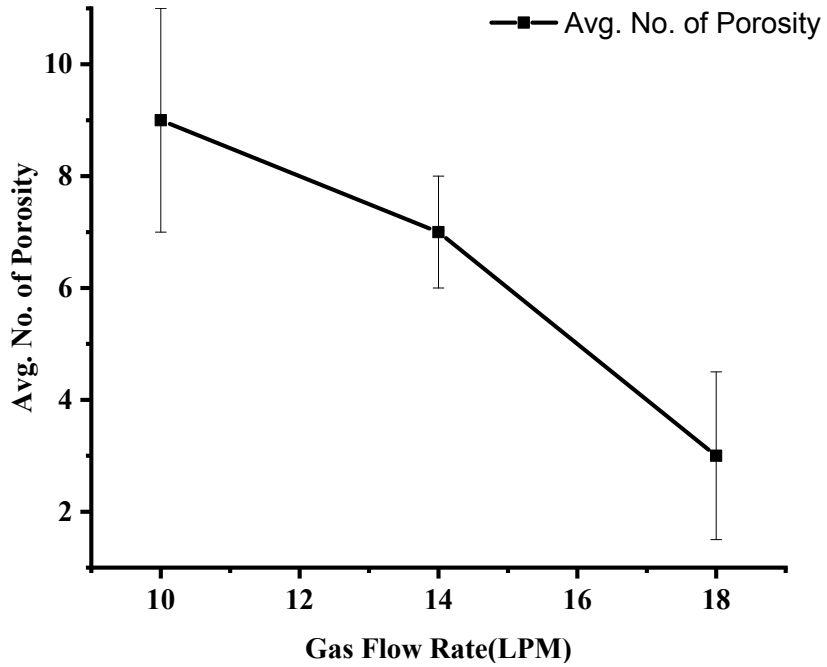

Figure 4.4: Average porosity at different gas flow rate

With these findings, the graph was plotted between the gas flow rate and percentage of porosity, as shown in Fig. 4.4. From the graph, it is concluded that the gas flow rate produced a reduction in the percentage of porosity compared with the argon base case that has been attributed to an increase in weld pool fluidity (Fortain et al.2013,Goyal et al.2009) It can also be noted that the percentage of porosity is found to reduce further through the application of another type of gas flow rate, 14 LPM. 10LPM is higher as compared to 18LPM and 14LPM.

Increase of the fluidity of weld pool helps in escaping of hydrogen gas bubbles, which may be the cause of weld porosity in weld pool. This is also evident from other investigations (Matsuda et al. 1978)

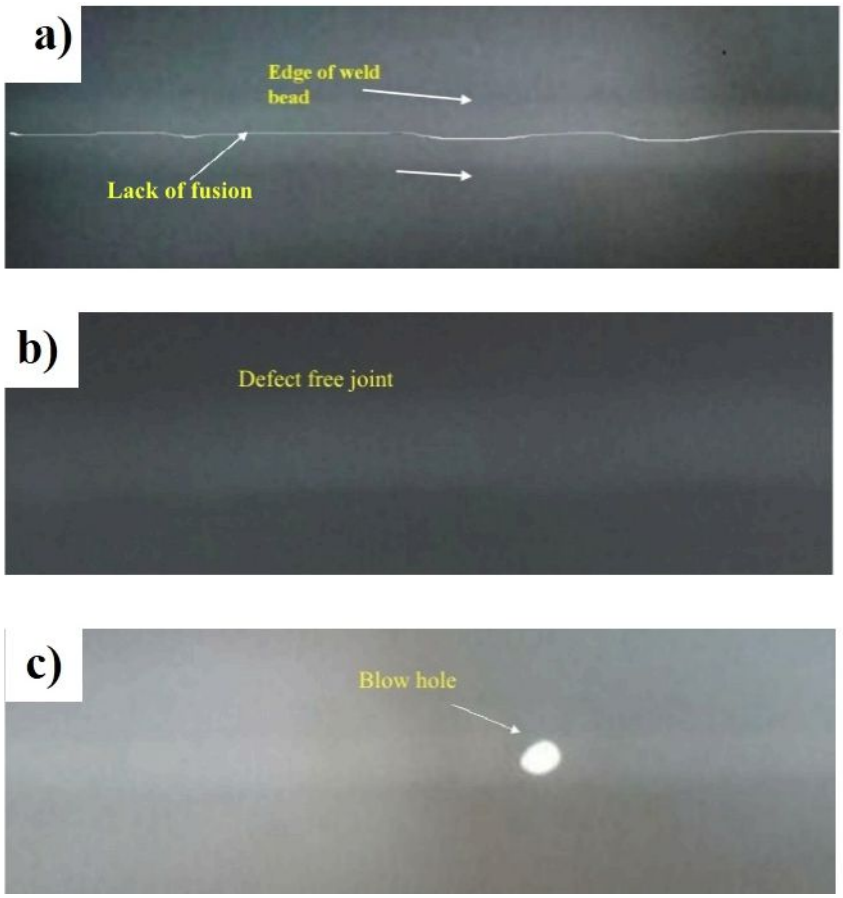

Figure 4.5: Radiography image at different gas flow rate a) 10 LPM b) 18 LPM, and c) 14 LPM

This higher heat input resulted in a reduced solidification rate, which allows the gas bubbles to escape from the weld pool area (Ambriz et al., 2014. This is also evident from other investigations (Kang et al., 2009) demonstrated that the gas flow rate could reduce the porosity present in the welding of A6061 and A6063 aluminium alloy.

4.5 Effect of Welding Parameters on Microstructure

The metallurgical micrographs can be used to clearly depict various zones such as fusion zones, HAZs and BMs, which provides valuable information about the changes that occur during welding. Uniformity across the joint and grain size can be directly correlated with the weldability of aluminium alloys joints. In welded joints heat input plays an important role in the formation of various types of microstructure in weld bead, fusion

zone and heat affected zone. Microstructural feature in weld bead and HAZ is primarily governed by Heat input. Primarily with current and further with weld speed per unit length. Shielding gas influences the total heat input in the weld pool as it, along with protection from oxidation, also removes the heat and ultimately affects the metallurgy of the weld joint. With an increase in heat input, there was a change in microstructure as well it can be evident from the morphology of weld bead and HAZ from the microstructure. The most influencing parameter has been current, and it governs the total heat imparted in the welding

4.5.1 Microstructure of A6061

The microstructure in the fusion zone of samples of MIG welded A6061 and A6063 aluminium alloy with different welding parameters is considerably affected by total heat imparted to the joint. The optical microstructure of the welded A6061 alloy was examined at different locations with respect to the surface, as shown in Fig. 3a-b. Typically elongated grains were observed in T-6 rolled A6061 plate (figure 3 a). The Heat affected zone characterized by coarse and irregular grains with uniformly distributed very fine precipitates (Fig. 3b). Fusion zone of MIG welded A6061 mostly contained dendritic structure due to the rapid heating and cooling of base metal and molten metal due to weld heat and high thermal conductivity. The Unaffected zone, heat affected zone and fusion zone of joint welded at Current: 160A, Voltage: 18V and Gas flow rate: 14LPM has been shown in Fig. 4.6(a-d). The only difference between the characteristic fusion zones are the dendrite arm spacing, which mainly attributes to heat input during the welding. The spacing is marginally higher as the heat input increases. The finer precipitates were uniformly distributed (Fig. 3 c, d, e) in the fusion zone. The precipitate coarsening was also observed as the heat input increases. All the weld zones exhibit an equiaxial crystal structure and show at weld fine grains of Al-Si- Mg eutectic particles in a matrix of Al

solid solution. The microstructure clearly shows grains of joint made by heat input are much finer and more uniform than those obtained by different welding conditions. Fine grains distinctly reduce the susceptibility of the weld metal to solidification cracking during welding. Fine grains will also enhance the mechanical properties of the weld. During welding, argon as shielding gas draws higher current and produces higher arc pressure due to its ionization characteristics (Kang et al. 2006, Marya et al. 2004). It is reported that a high current will likely result in a higher arc force, and a low current will likely result in a lower arc force (Rokhlin et al. 1993). The weld pool surface will rise and fall as the arc force regularly changes during the supply of shielding gas, thereby enhancing the stirring effect on the weld pool. This phenomenon produces intense weld pool convection (Becker1979). The microstructure of base materials A6061 and A6063 can be seen in Fig. 4.7 and Fig. 4.24, respectively.

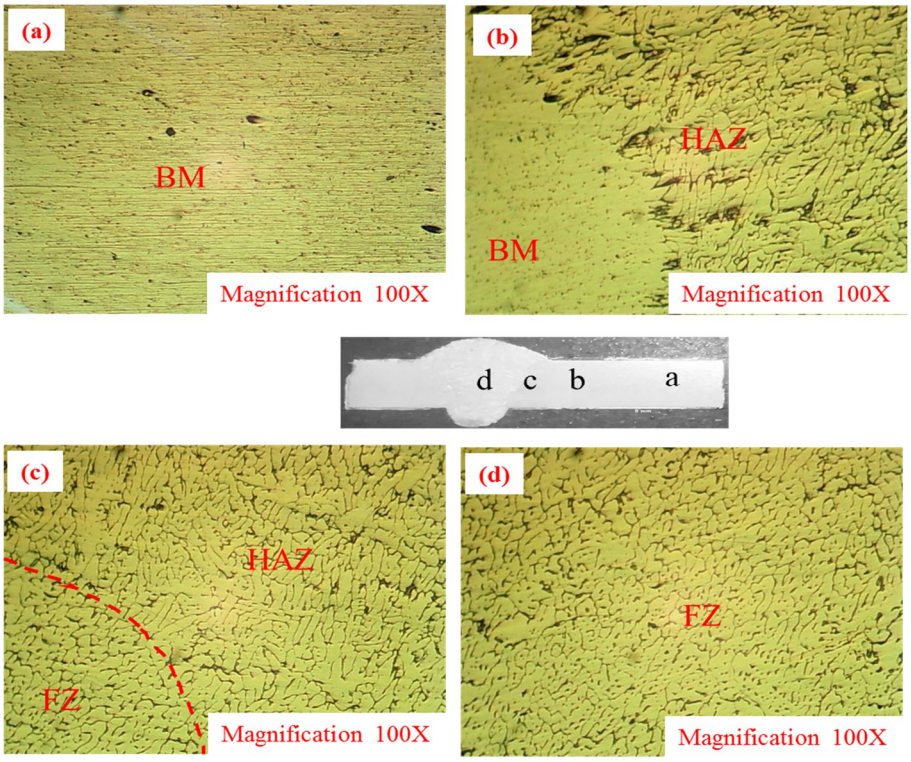

Fig. 4.6: Optical Micrographs welded A6061 alloy for Welding Parameter: Current: 160A Voltage:18V Gas flow rate: 14LPM: (a) Base metal(BM) (b) Transition zone(TM),(c) Fusion line(FL)(d) Fusion Zone(FZ)

Further, it can be observed from the micrograph of welded joint welded at Current: 160A Voltage: 18V Gas flow rate: 14LPM and HI: 9.2 kJ/cm the base metal has shown similar features, and the region is unaffected by weld heat, i.e. No microstructural changes occur in this zone for all the samples welded.

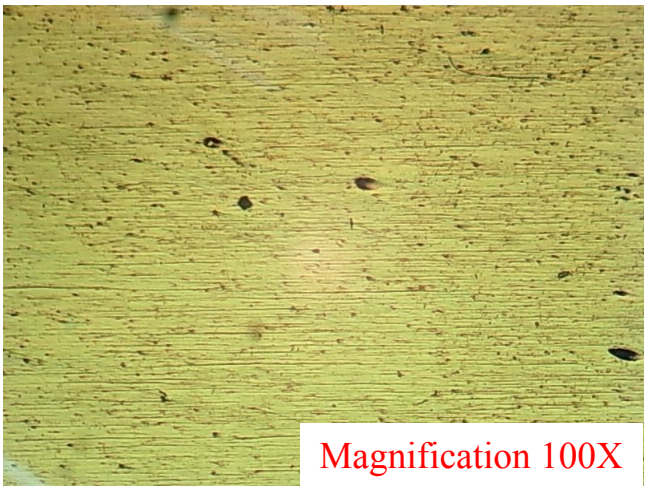

Figure 4.7: BM: Region is un-affected by weld heat Current: 160A Voltage:18V Gas flow rate: 14LPM, HI: 9.2 kJ/cm

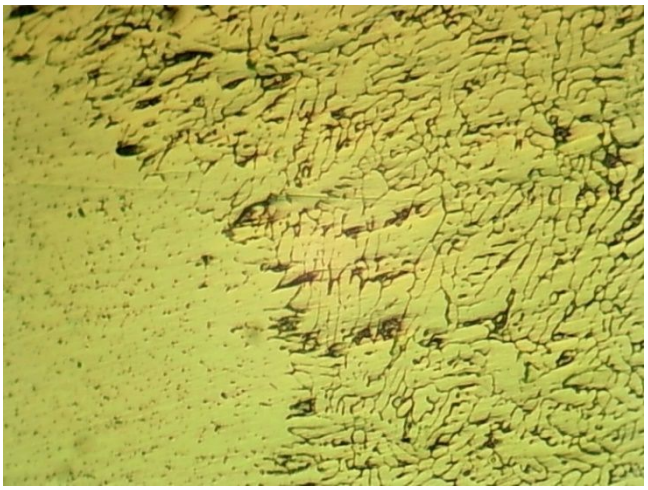

Figure 4.8: Optical micrograph of MIG welded A6061 alloy: Transition zone(TM) Current: 160A Voltage: 18V Gas flow rate: 14LPM, HI: 9.2 kJ/cm

Fig: 4.8 Optical micrograph of MIG welded A6061 alloys: Transition zone(TM) representing a clear distinguishing line for BM and HAZ for Welding Parameter: Current: 160A Voltage: 18V Gas flow rate: 14LPM having HI: 9.2 kJ/cm

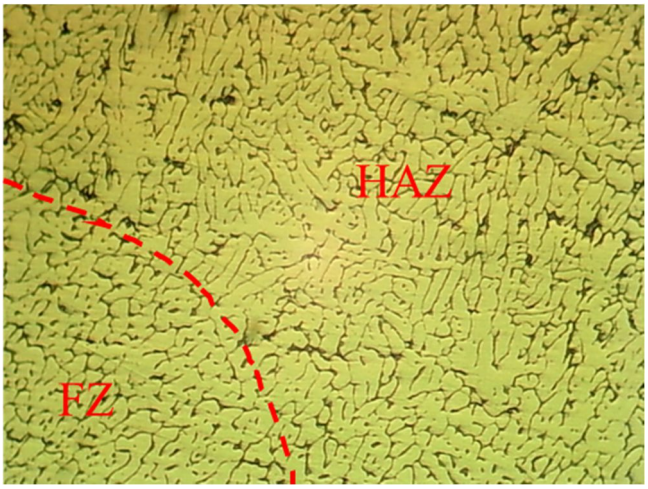

Figure 4.9: Optical micrograph of MIG welded A6061 alloys: Fusion line(FL)

Optical micrograph of MIG welded A6061 alloys: Fusion line(FL) from Fig: 4.9 it can be seen that HAZ zone affected by thermal cycle has columnar grains that grow from FZ and have coarse grain due to lower cooling rate (Welding Parameter: Current:160A, Voltage:18V Gas flow rate: 14LPM HI: 9.2 kJ/cm) Fusion Zone(FZ) has equiaxed grains due to high cooling rate (Welding Parameter:Current:160A Voltage:18V Gas flow rate: 14LPMand HI: 9.2 kJ/cm).

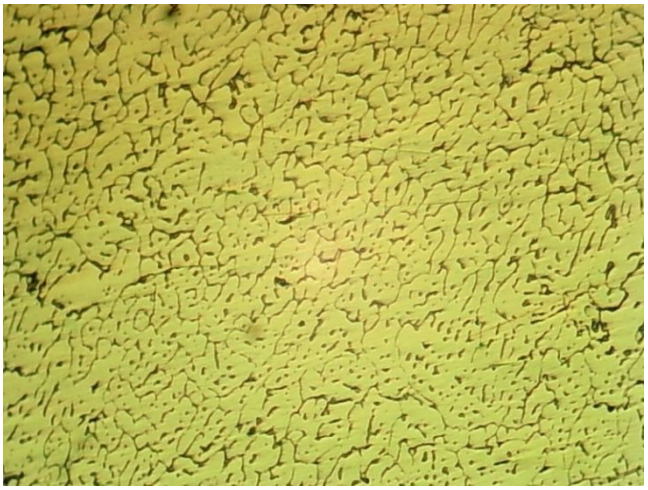

Figure 4.10: Optical micrograph of MIG welded A6061 alloy: Fusion Zone (FZ)

For Gas flow rate of 10LPM and different heat input the microstural changes can be seen in Fig. 4.11(a), 4.12(b), 4.13(c) and 4.14(d). Welding Heat Inputs for in Fig. 4.11(a),

4.12(b), 4.13(c) and 4.14(d) are a)6.7kJ/cm, (b)9.4kJ/cm, (c)8.6kJ/cm and (d)12.1kJ/cm respectively. With increase in Heat Input there is grain growth in Weld metal as well as more precipitation dissolution occurs.

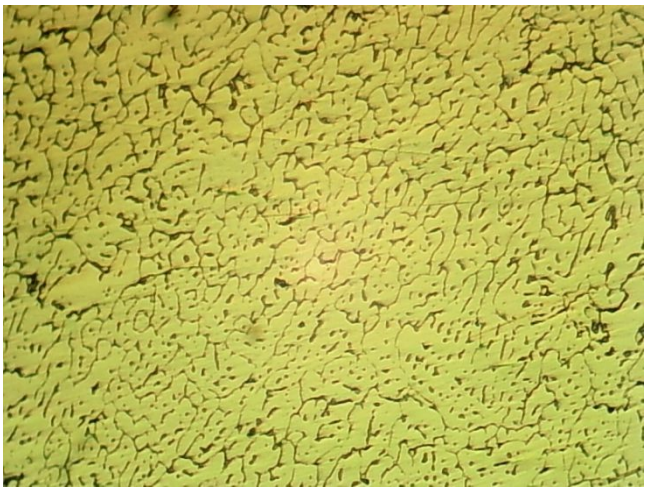

Figure 4.11: Optical micrograph (a) 140A_15V at Gas flow rate: 10LPM and Heat Input of (a) 6.7kJ/cm

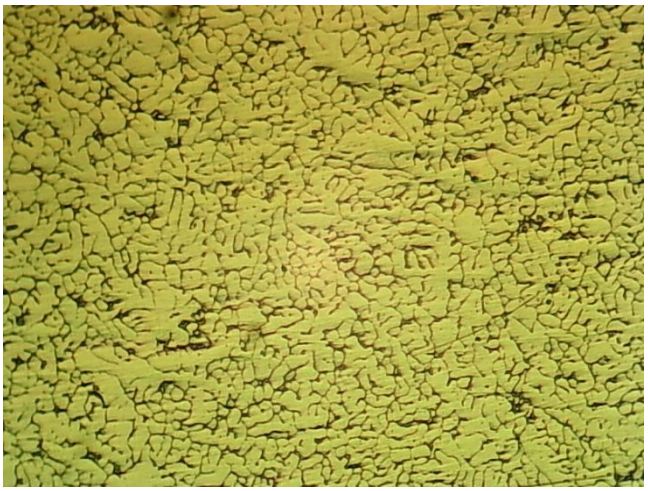

Figure 4.12: Optical micrograph (b) 140A_21V at Gas flow rate: 10LPM and Heat Input of (b) 9.4kJ/cm

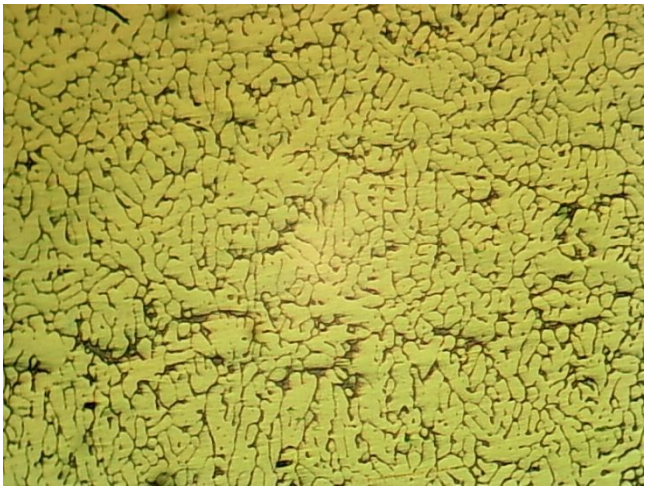

Figure 4.13: Optical micrograph(c) 180A_15V at Gas flow rate: 10 LPM and Heat Input of (c) 8.6kJ/cm

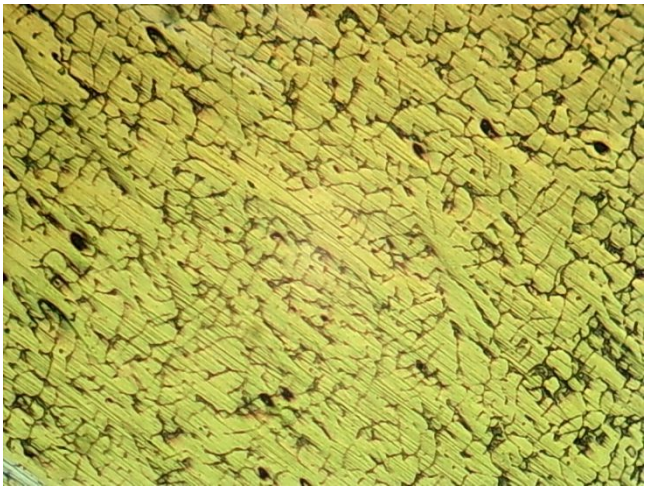

Figure 4.14: Optical micrograph (d) 180A_21V at Gas flow rate: 10LPM and Heat Input of (d) 12.1kJ/cm

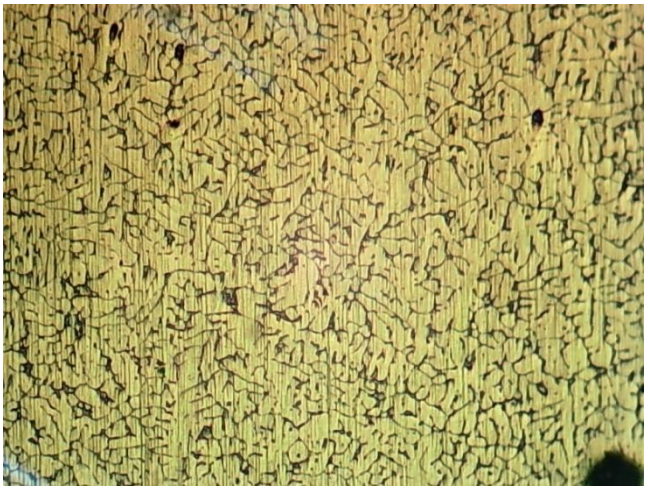

Figure 4.15: Optical micrograph (a) 140A_15V at Gas flow rate:14 LPM and Heat Input of(a)6.7kJ/cm

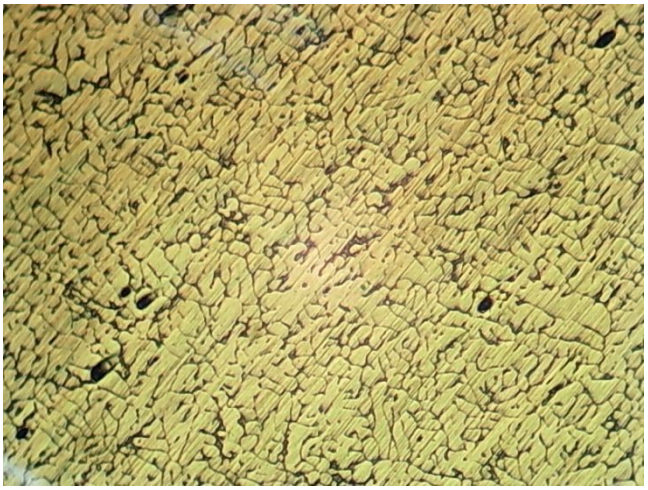

Figure 4.16: Optical micrograph (b) 140A_21V at Gas flow rate:14 LPM and Heat Input of(b)9.4kJ/cm

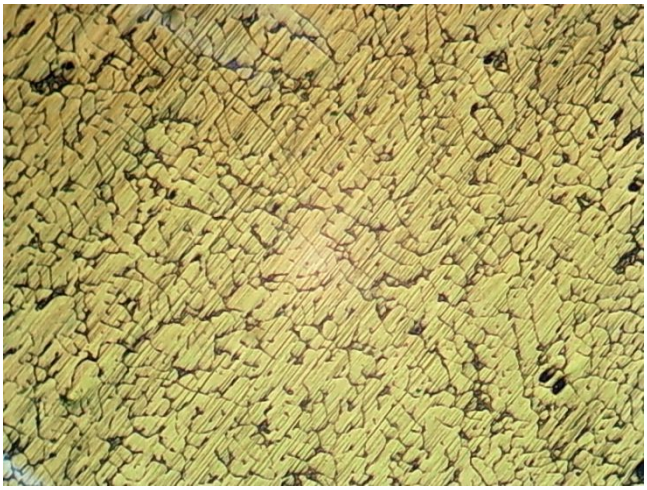

Figure 4.17: Optical micrograph (c) 180A_15V at Gas flow rate:14 LPM and Heat Input of (c)8.6kJ/cm

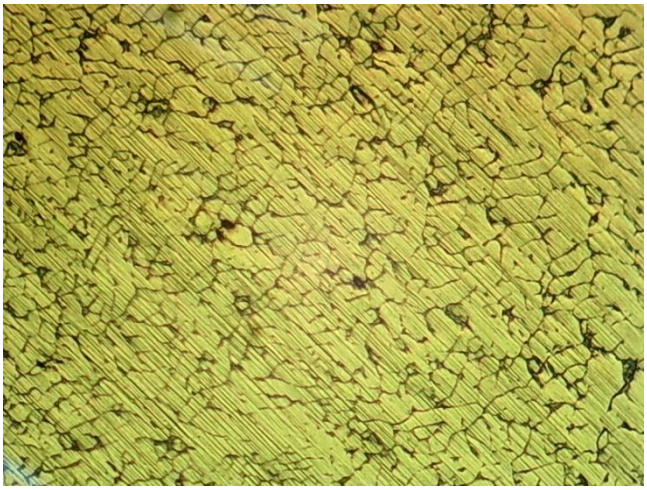

Figure 4.18: Optical micrograph (d)180A_21V at Gas flow rate:14 LPM and Heat Input of (d)12.1kJ/cm

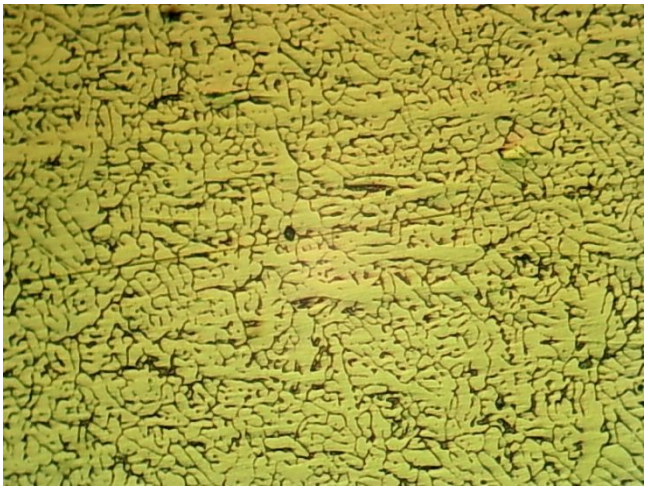

Figure 4.19: Optical micrograph (a) 140A_15V at Gas flow rate: 18 LPM and Heat Input of (a) 6.7kJ/cm

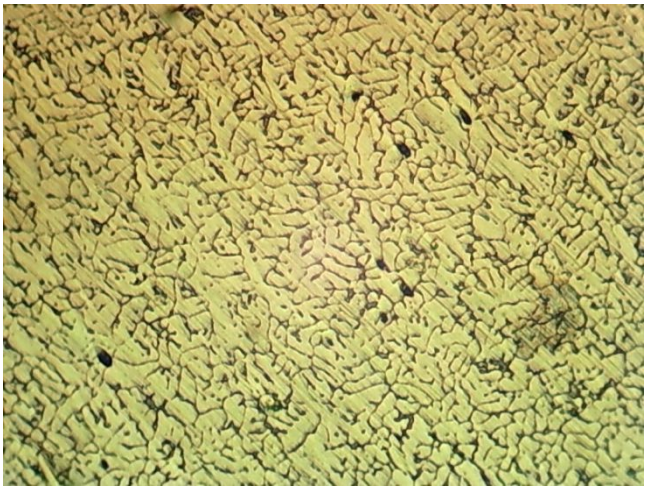

Figure 4.20: Optical micrograph (b) 140A_21V at Gas flow rate: 18 LPM and Heat Input of (b) 9.4kJ/cm

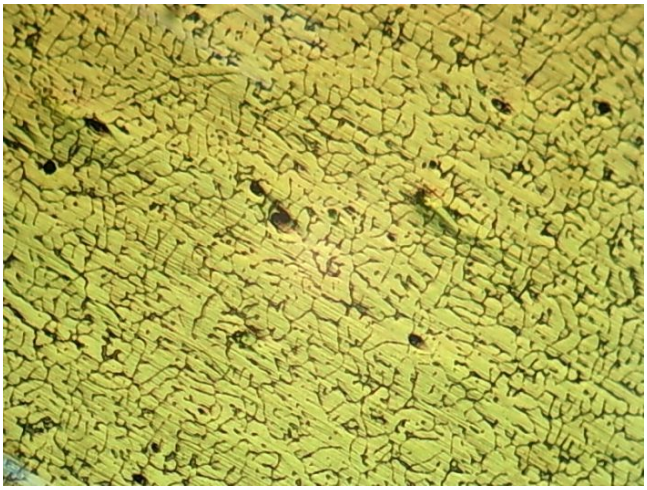

Figure 4.21: Optical micrograph (c) 180A_15V at Gas flow rate: 18 LPM and Heat Input of (c) 8.6kJ/cm

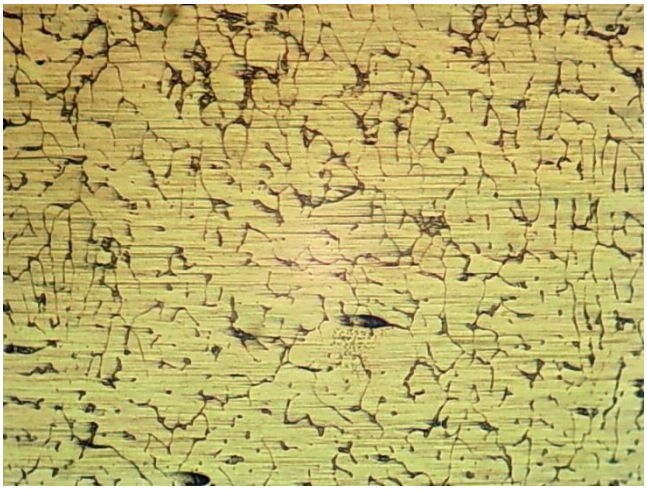

Figure 4.22: Optical micrograph (d) 180A_21V at Gas flow rate: 18 LPM and Heat Input of (d) 12.1kJ/cm

4.5.2 Microstructure of A6063

The microstructure in the fusion zone of samples of MIG welded A6063 aluminium alloy with different welding parameters current-voltage gas flow rate by heat input. All the weld zones exhibit an equiaxial crystal structure and show at weld fine grains of Al-Si- Mg eutectic particles in a matrix of Al solid solution. The microstructure clearly shows grains of joint made by heat input are much finer and more uniform than those

obtained by different welding conditions. Fine grains distinctly reduce the susceptibility of the weld metal to solidification cracking during welding. Fine grains will also enhance the mechanical properties of the weld. During the supply of argon, shielding gas draws higher current and produces higher arc pressure due to its ionization characteristics, (Kang et al. 2006. Marya et al. 2004. It is reported that a high current will likely result in a higher arc force and a low current will likely result in a lower arc force (Rokhlin et al. 1993). The weld pool surface will rise and fall as the arc force regularly change during the supply of shielding gas, thereby enhancing the stirring effect on the weld pool. This phenomenon produces intense weld pool convection (Becker1979).

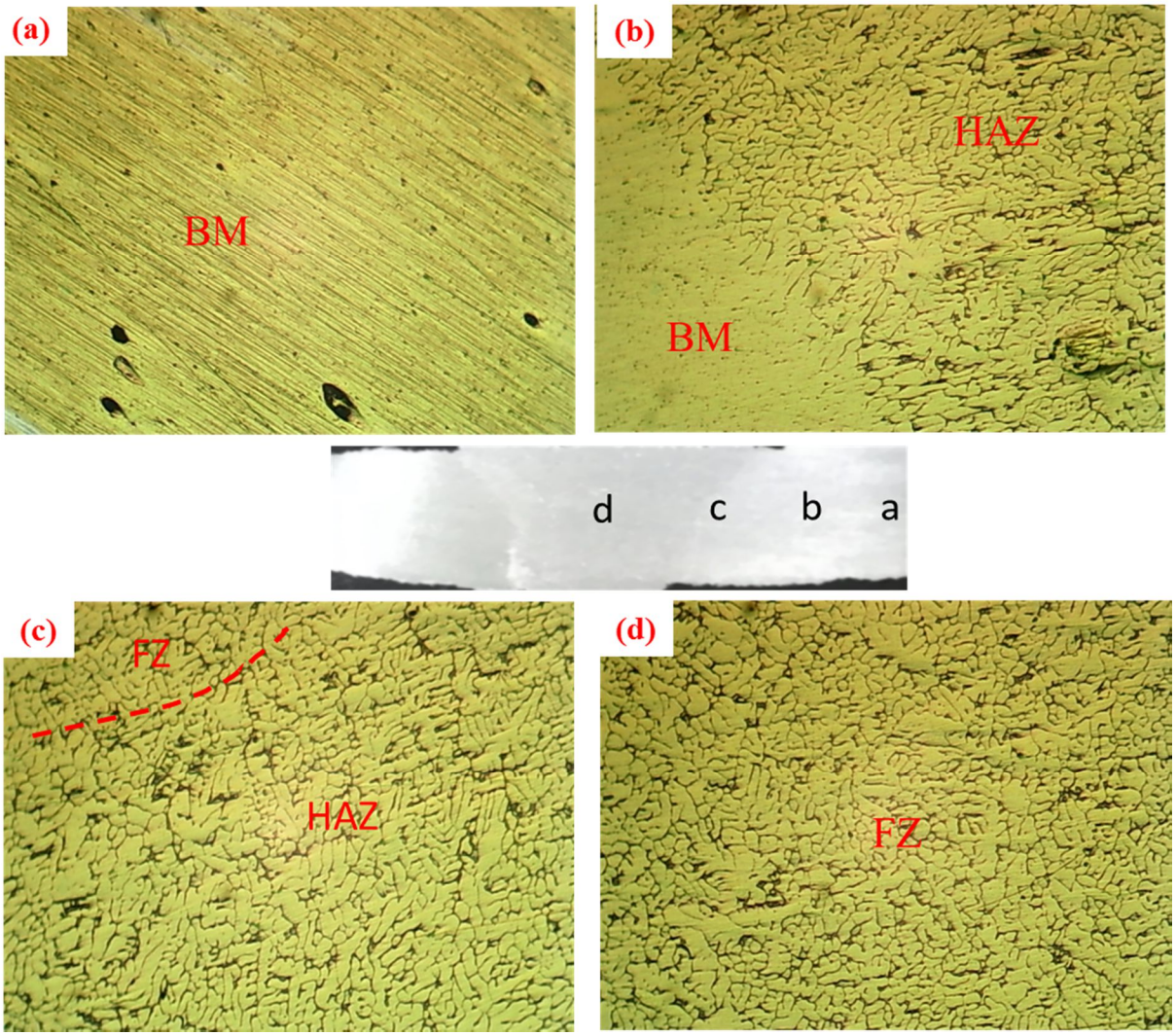

Figure 4.23: Optical Micrographs welded A6063 alloy for Welding Parameter: Current: 160A Voltage:18V Gas flow rate: 14LPM: (a) Base metal(BM) (b) Transition zone(TM),(c) Fusion line(FL)(d) Fusion Zone(FZ)

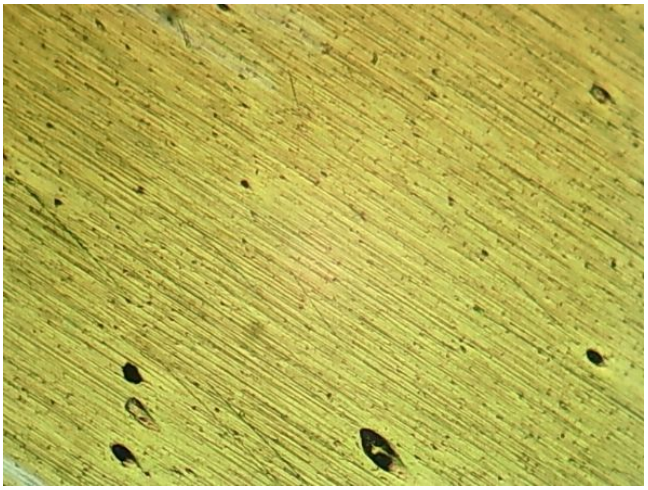

Figure 4.24: BM: Region is un-affected by weld heat

Optical micrograph of MIG welded A6063 alloy shows BM region which is un-affected by weld heat i.e. No microstructural changes occur in this zone for Welding Parameter: Current:160A Voltage:18V Gas flow rate:14LPM HI: 9.216kJ/cm

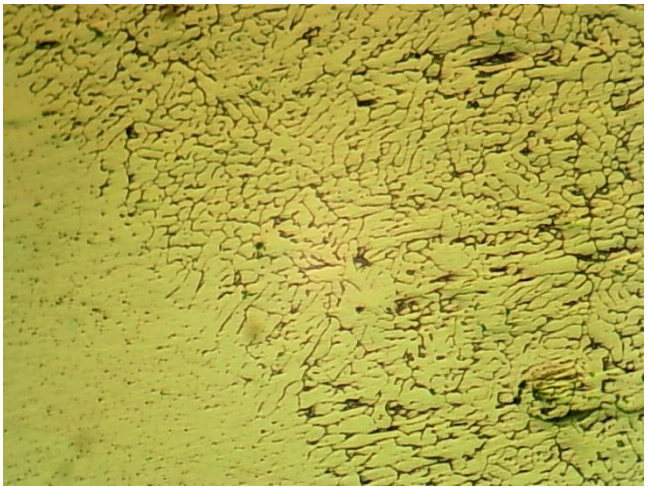

Figure 4.25: Optical micrograph of MIG welded A6063 alloy: (b) Transition zone(TM)

Fig. 4.26 shows the distinguishing line for BM and HAZ for Welding Parameter: Current: 160A Voltage:18V Gas flow rate:14LPM HI: 9.216kJ/cm

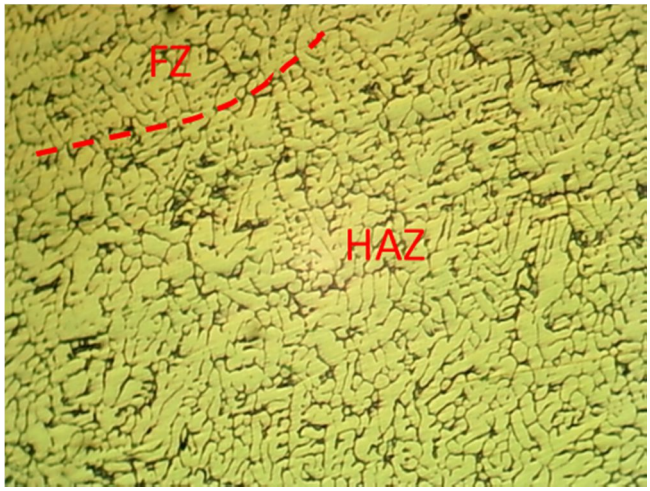

Figure 4.27: Optical micrograph of MIG welded A6063 alloy: (c) Fusion line (FL)

HAZ zone affected by thermal cycle during welding has columnar grains that grow from FZ and have coarse grain due to lower cooling rate for Welding Parameter: Current:160A Voltage:18V Gas flow rate:14LPM HI: 9.216kJ/cm

Figure 4.28: Optical micrograph of MIG welded A6063 alloy (d) Fusion Zone(FZ)

From the optical micrograph of MIG welded A6063 alloy the Fusion Zone (FZ) has equiaxed grains due to sufficient time for solidification FZ mainly composed of α-Al phases and dispersed Mg2Si precipitates which was confirmed through XRD analysis.

Figure 4.29: Optical micrograph (a) 140A_15V at Gas flow rate: 10LPM and Heat Input of (a) 6.7kJ/cm

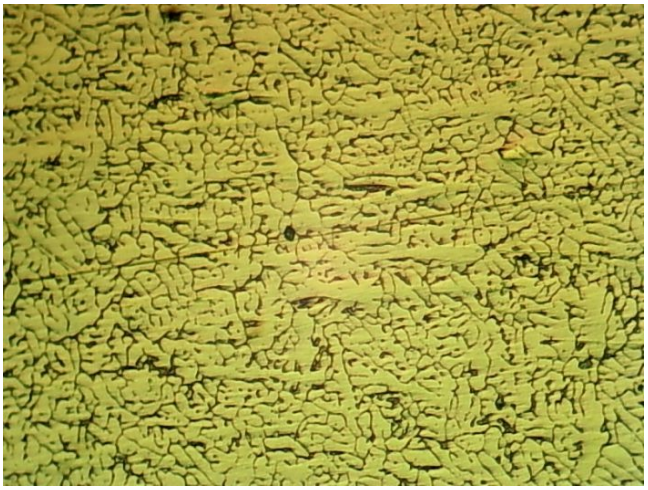

Figure 4.30: Optical micrograph (b) 140A_21V at Gas flow rate: 10LPM and Heat Input of (b) 9.4kJ/cm

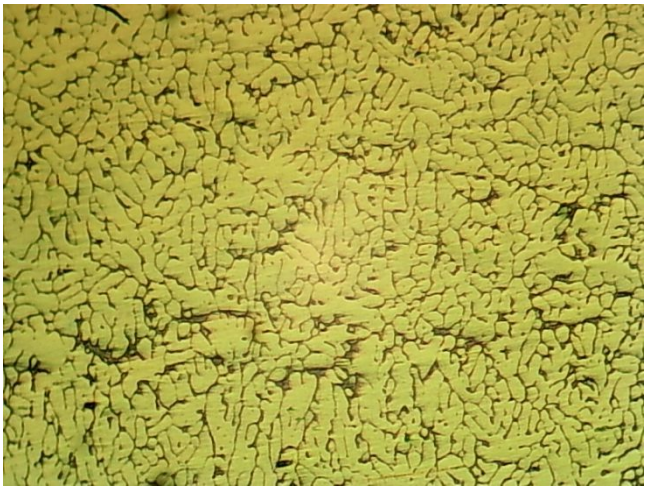

Figure 4.31: Optical micrograph (c) 180A_15V at Gas flow rate: 10LPM and Heat Input of (c) 8.6kJ/cm

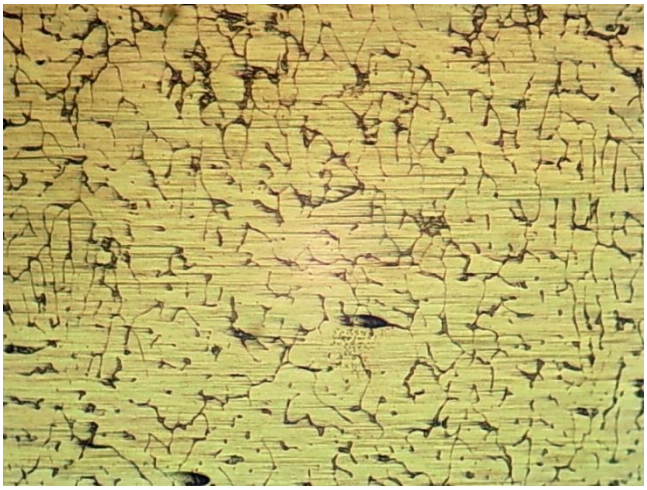

Figure 4.32: Optical micrograph (c) 180A_21V at Gas flow rate: 10LPM and Heat Input of (d) 12.1kJ/cm

Figure 4.33: Optical micrograph (a) 140A_15V at Gas flow rate: 14LPM and Heat Input of (a) 6.7kJ/cm

Figure 4.34: Optical micrograph (b) 140A_21V at Gas flow rate: 14LPM and Heat Input of (b) 9.4kJ/cm

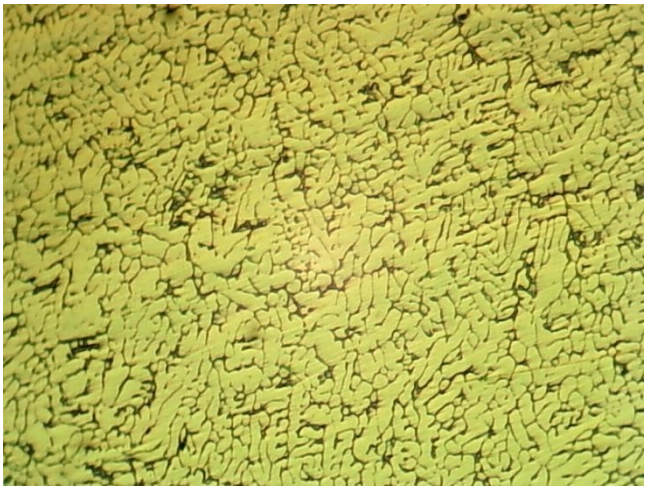

Figure 4.35: Optical micrograph (c)180A_15V at Gas flow rate: 14LPM and Heat Input of (c)8.6kJ/cm

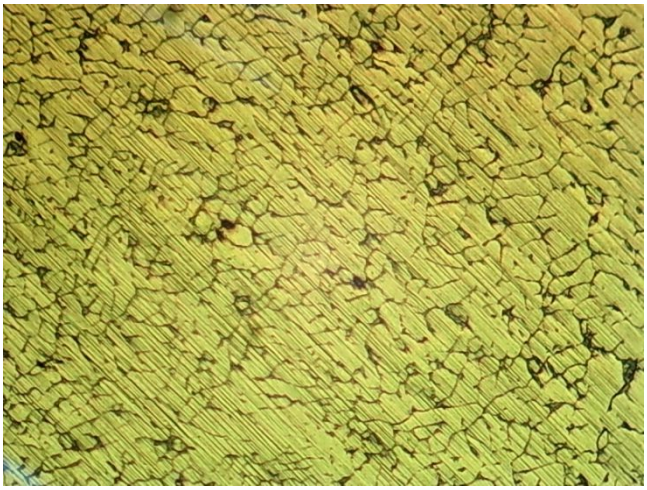

Figure 4.36: Optical micrograph (d) 180A_21V at Gas flow rate: 14LPM and Heat Input of (d)12.1kJ/cm

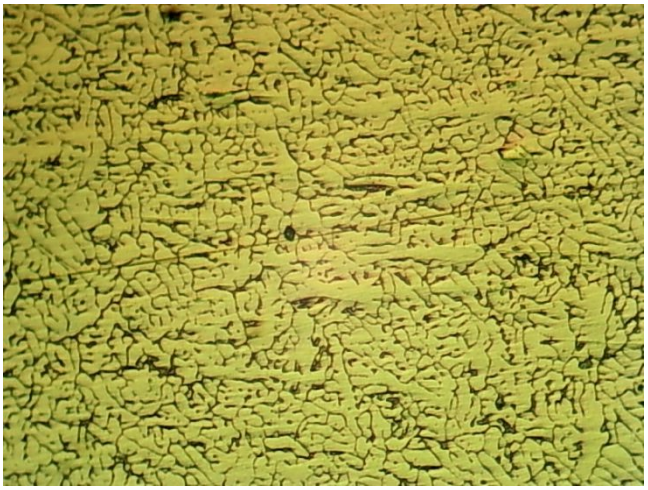

Figure 4.37: Optical micrograph (a) 140A_15V at Gas flow rate: 18LPM and Heat Input of (a)6.7kJ/cm

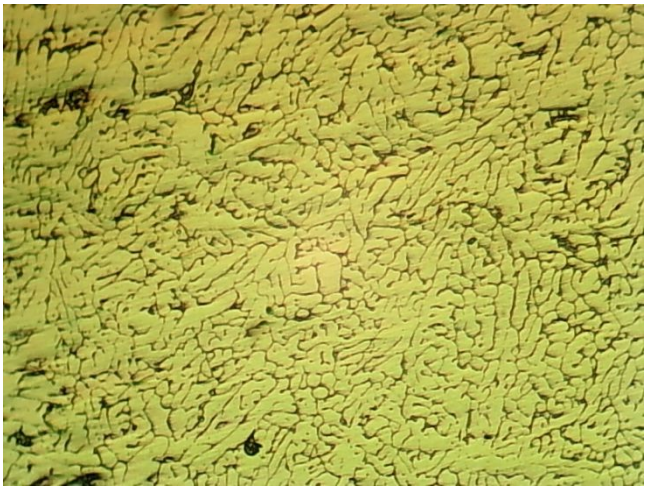

Figure 4.38: Optical micrograph (b) 140A_21V at Gas flow rate: 18LPM and Heat Input of (b) 9.4kJ/cm

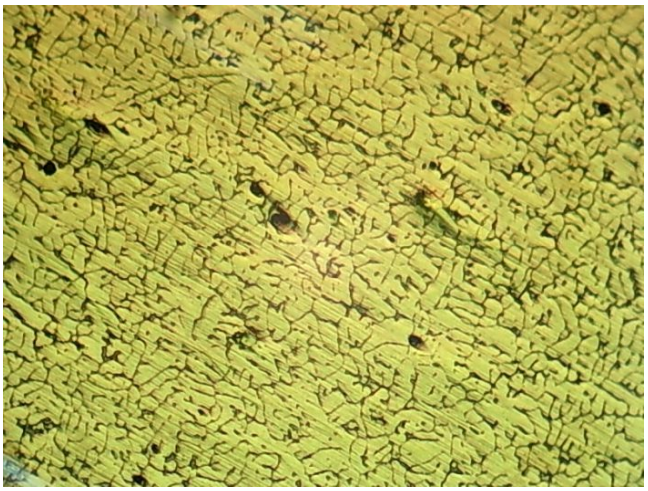

Figure 4.39: Optical micrograph (c) 180A_15V at Gas flow rate: 18LPM and Heat Input of (c) 8.6kJ/cm

Figure 4.40: Optical micrograph (d) 180A_21V at Gas flow rate: 18LPM and Heat Input of (d)12.1kJ/cm

The weld pool convection process will lead to the molten metal moving forward and back in the weld pool at a certain frequency. The solidification process is affected, and in the meantime, the grain growth is inhibited due to scouring and shearing. As a result, the grain growth is hindered, and the broken grains become the nucleation sites for new grains (Wang et al. 2016).

The magnified microstructures of the weld metal as-welded joint joints were given in Fig. 4.7. The micrograph of weld metal presents an equiaxed dendritic network. Fine weld metal microstructure is attributed to fast cooling rates in the associated weld. After welding, we have to consider the fusion zone, were melting and re-solidification occur, and a zone deteriorated by the heat of the welding process (Temmar et al. 2012).

The weld metal of the as-welded joint was covered with precipitated particles which caused the grain boundary not clear. Solution treatment followed by aging formed a supersaturated solid solution, beginning the precipitation of strengthening particles in the matrix. The higher values of hardness and tensile strength and elongation are since Heat

Input produces a fine and uniform distribution of precipitates at the weld joints (Ahmad et al. 2011).

4.5.3 Grain Size Distribution and Phase Transformation

During the supply of shielding gas Ar to the welding torch, due to its ionization properts it draws higher current and produces higher arc pressure (Kang et al. 2006, Marya et al. 2004). Arc pressure is higher when Ar passes the torch. The changes in arc pressure cause changes in the weld pool movement. The temperature of weld pools changes due to the turbulent action of the weld pool during the gas flow rates. This phenomenon favors the formation of a typical rippling appearance on the welding joint, as well as enhances the flow of weld pools to produce a more uniform and finer microstructure (Shufen et al.2014). Therefore, the current difference that occurred during the gas flow rates plays an important role in the microstructure transformation.

The changes in arc pressure occurred during the various gas flow rates not only improves the uniformity of alloy element distribution but also disturbs the coarse columnar grains into small grains due to the stirring effect on the weld pools, both of which influence the microstructure of the welding joint and promote the heterogeneous nucleation in the solidification process of weld pools (Yang et al. 2005). During the solidification of molten metal in the weld, grains nucleated on the surface of the unmelted metal and grew toward the center of the weld. Meanwhile, the equiaxed grains formed in the center of the weld. Generally, the higher the pressure difference, the more uniform and finer microstructure attained on the welding joint (Fig. 4.7 a, c and e).

The finer and more uniform grains in the FZ are due to the strong arc stirring effect which could lead to grains refinement, and this will benefit the property of the welded bead. The addition of the Si improved significantly the weld joint hardness (Zhao et al.

2009). Due to its high strength and hardness, the eutectic phase Mg2Si can improve the strength of the fusion zone significantly. It illustrates that the fusion zone primarily consisted of Al and eutectic phase Mg2Si. The Si and Mg elements were from rich-Si filler wire and rich-Mg base material, respectively. After the eutectic reaction in the weld pool, the Mg2Si phase precipitated uniformly along the grain boundaries and forms a network. That results in a significant enhancement of the mechanical properties of the fusion zone (Usta et al. 2004).

The higher arc pressure obtained during the 14LPM gas flow rate resulted in fine and uniform microstructure as compared to the 10LPM, 18LPM gas flow rates of pure argon. The turbulent molten metal flow that occurred during gas flow rates accelerated the gases to escape from the molten metal. Another point that would make the gas entrapment lower in welds is the breakage of the columnar growths during the gas flow rates, reducing the grain size and splitting the pores between them.

From the result of microstructure analysis of gas flow rates welded joints, there is significant variation in size and distribution in strengthening particles. Finer and uniform distributed precipitates were seen in 14LPM gas flow rate welded joints, compared to as gas flow rates 10LPM, 18LPM welded joints, and the dislocation density was higher for 14LPM gas flow rate joints compared to as welded joints. Solution treatment followed by artificial aging, the precipitate was very fine and uniformly distributed at 14LPM gas flow rate welded region in (Fig. 4.7(a), (b), (c), and (d). This phenomenon can be explained by the effect of artificial aging.

It is because of Mg and Si as main components of the 6xxx series Aluminium alloy and 6xxx obtained its strength from the precipitation hardening, due to MgSi (Tan et al.

2007 and Sivaraj et al. 2014). This is the reason for the higher hardness and superior tensile properties of the different heat inputs of A6061 and A6063 alloy.

4.6 XRD Analysis of Welded Joint

4.6.1 XRD Analysis of A6061

The effect of heat input on phase formation can be studied using XRD analysis. XRD analyses were carried out at the weld region of the joint specimen to identify the phase formation for heat input. The harder Mg2Si precipitate formed during the welding, and it was observed by XRD peaks (Fig.4.40). The finer precipitates were uniformly distributed in the fusion zone. The precipitate coarsening was also observed as the heat input increases. FZ mainly composed of α-Al phases and dispersed Mg_2Si precipitates which were revealed from XRD analysis.

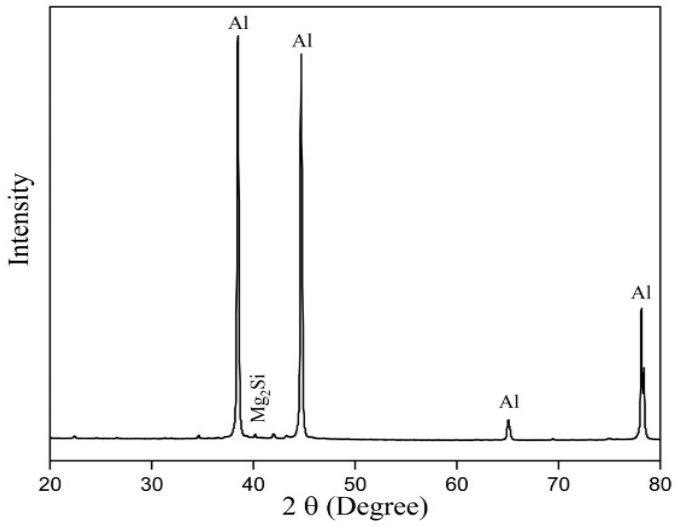

Figure 4.41: XRD analysis of A6061 weld bead during welding

4.6.2 XRD Analysis of A6063

The harder Mg2Si precipitate formed during the welding, and it was observed by XRD peaks (Fig.4.41). The finer precipitates were uniformly distributed in the fusion zone. The precipitate coarsening was also observed as the heat input increases.

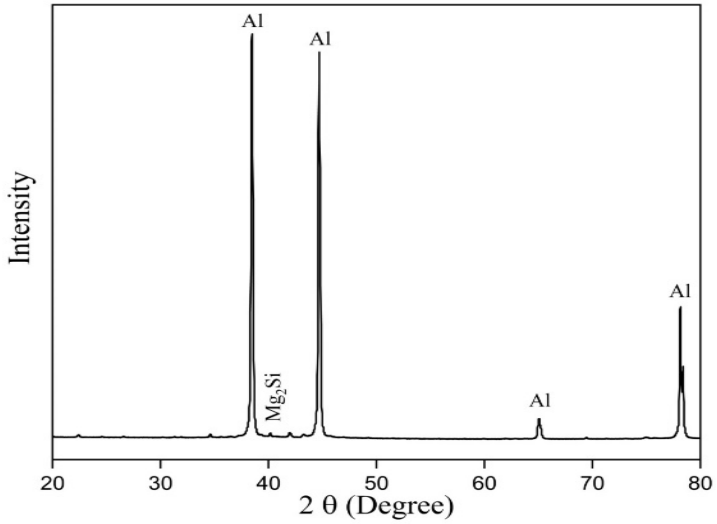

Figure 4.42: XRD analysis of A6063 weld bead during welding

4.7 Effect of Welding Parameters on Microhardness

Microhardness tests were carried out on each of the samples using a 0.03 kg weight. The distance between each indentation was set at 1mm in the weld region, heat affected zone region, and base metal region to have an idea of the hardness without the effects of work hardening in the surrounding areas of each indentation.

Microhardness test results of are illustrated in Fig. 4.6. In all cases of as-welded samples, hardness in the weld bead center was higher than in the heat-affected zone and base metal. As compared to gas flow rate the joint made by using 10LPM, 14LPM and 18LPM: Hardness of the weld metal is increased, from 81 to 85 and decrease 83 Hv respectively. Gas flow rate periodically increased the pressure of welding arc which resulted in grain refinement of weld metal structure (Novikov et al. 2013). Gas flow rates increased in thermal frequency. The hardness of the weld joint is improved with the increase of thermal frequency due to reduced porosity rate, refined grain size, and increased Mg_2Si precipitate (Wang et al. 2016).

4.7.1 Effect of Welding on Microhardness of A6061

The microhardness profiles for as-welded joints are shown in Fig.4.42 The microhardness of the as-welded joints. The variation in hardness can be attributed primarily to the heat input. The decrease in hardness value in the heat-affected zone due to coarser grain size is mainly attributed to the annealing effect. The higher value of hardness in the fusion zone due to the rapid cooling, influenced by the increased gas flow rate. Significantly hardened the welded joints in all zones and increase hardness value by 19.64%.

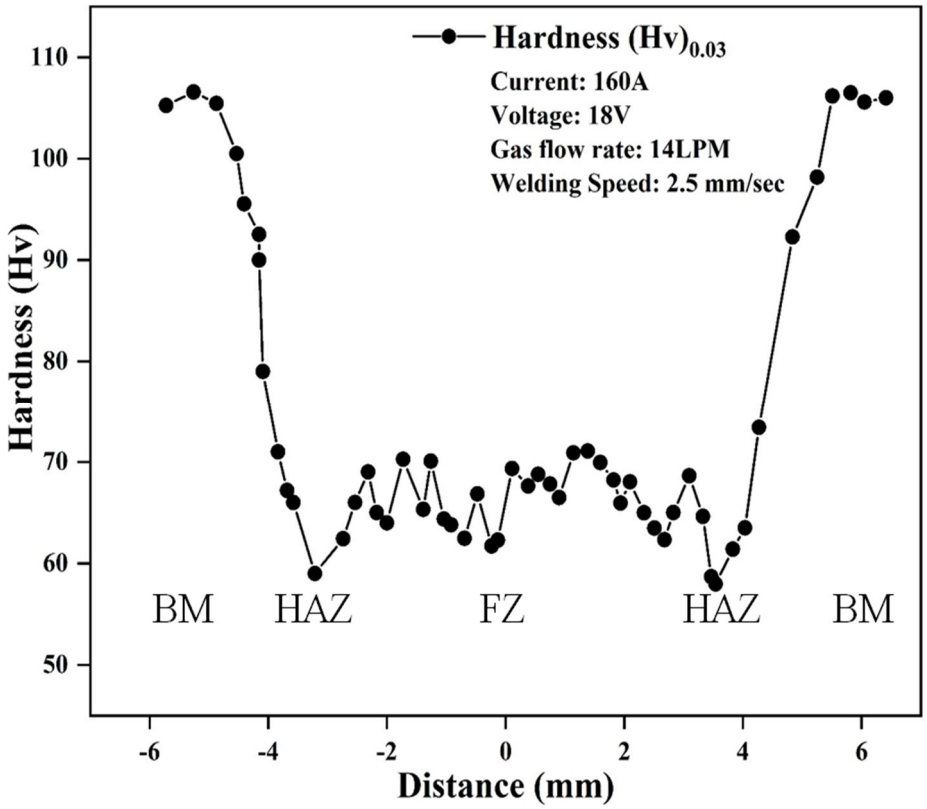

Figure 4.43: Variation of microhardness across weld of A6061 for Current: 160A, Voltage: 18V and Gas flow rate: 14LPM and different zones BM: Base Metal, HAZ: Heat Affected Zone FZ: Fusion Zone

The average hardness value of the fusion zone of MIG welded A6061 aluminium alloy having different current and voltage values at a constant gas flow rate (a) 10LPM has been

shown in Fig. 4.43. It was found that fine dimples increase the tensile strength and hardness. This was attributed to precipitation hardening in the weld metal region.

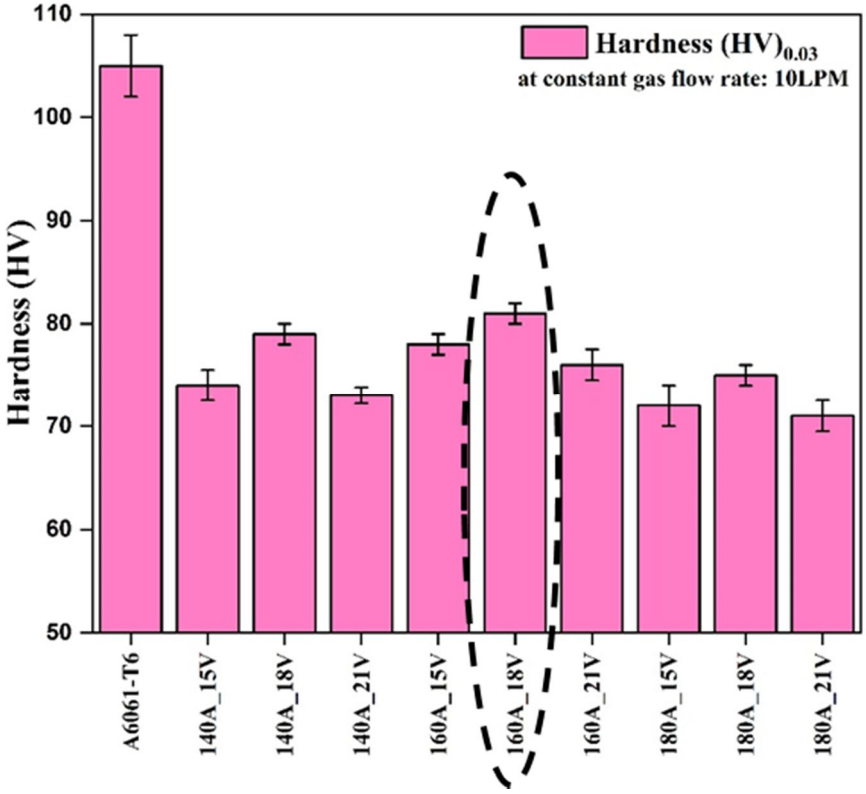

Figure 4.44: Microhardness distribution of A6061 for Fusion zones at gas flow rate of 10LPM

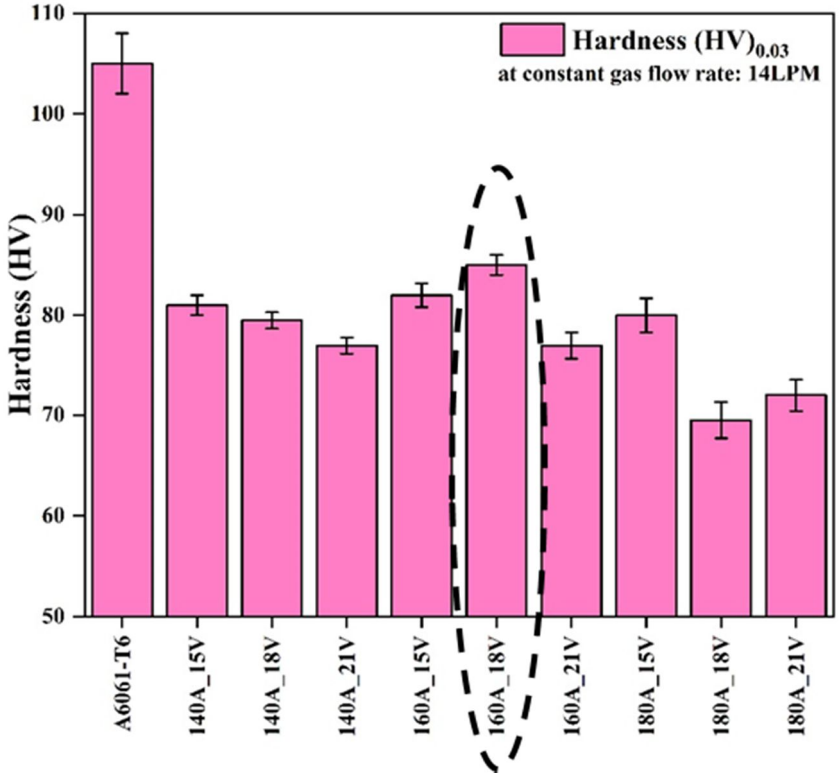

Figure 4.45: Microhardness distribution of A6061 for Fusion zones at gas flow rate of 14LPM

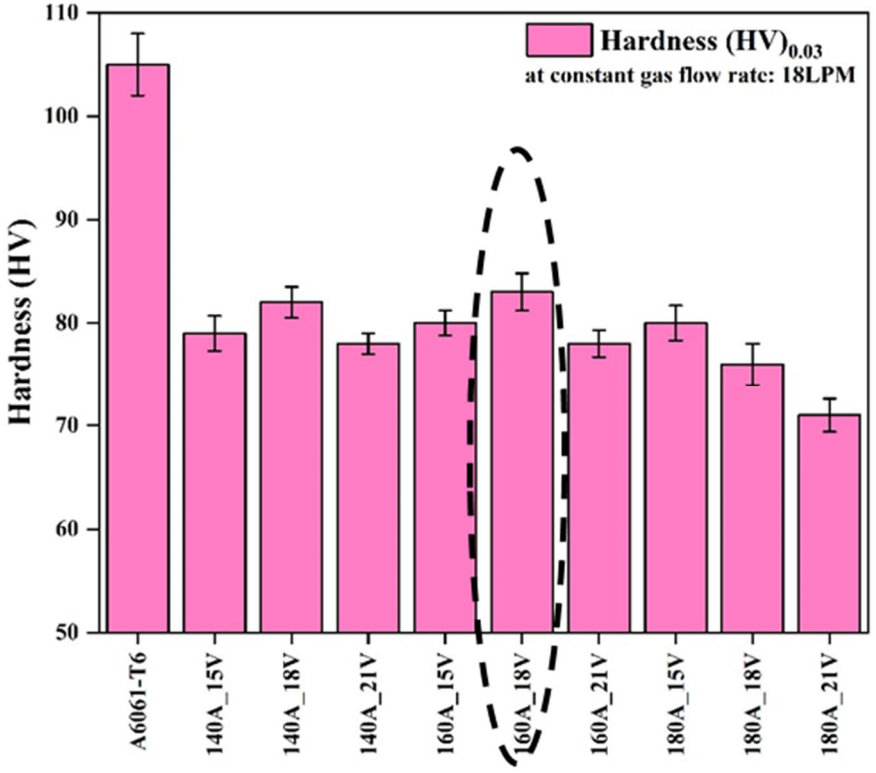

Figure 4.46: Microhardness distribution of A6061 for Fusion zones at gas flow rate of 18LPM

4.7.2 Effect of Welding on Micro Hardness of A6063

A similar variation in hardness of A6063 was observed in all the samples. The microhardness profiles for as-welded joints are shown in Fig. 4.46. The microhardness of the as-welded joints. The variation in hardness can be attributed primarily to the heat input. The decrease in hardness value in the heat-affected zone due to coarser grain size is mainly attributed to the annealing effect. Hardness distribution 2 mm below the surface and across weld of A6061 for Current: 160A, Voltage: 18V and Gas flow rate: 14LPM with respect to different zones BM: Base Metal HAZ: Heat Affected Zone FZ: Fusion Zone has been shown in Fig. 4.46 which shows lower bead hardness with respect to base material and HAZ(Shoo et al. 1988, Serdar et al. 2008).

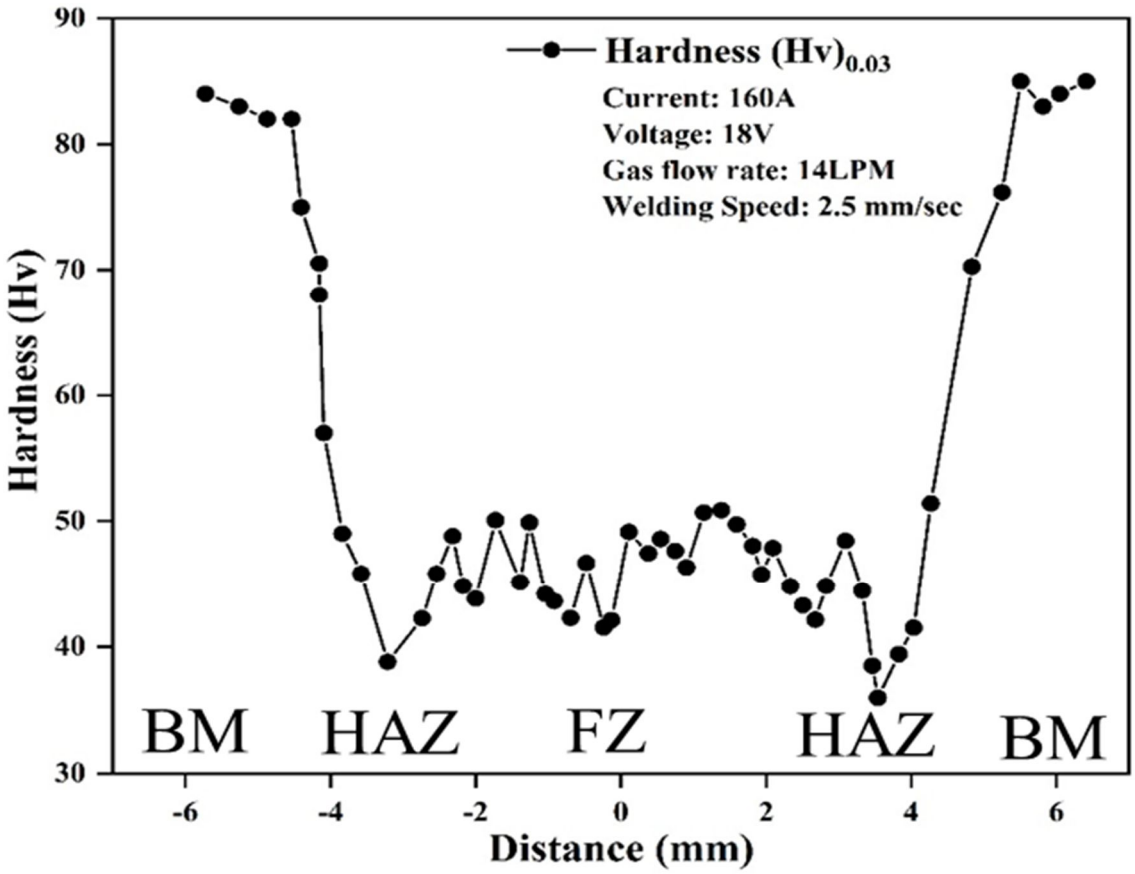

Figure 4.47: Variation of microhardness across weld of A6063 for Current: 160A, Voltage: 18V and Gas flow rate: 14LPM and different zones BM: Base Metal HAZ: Heat Affected Zone FZ: Fusion Zone

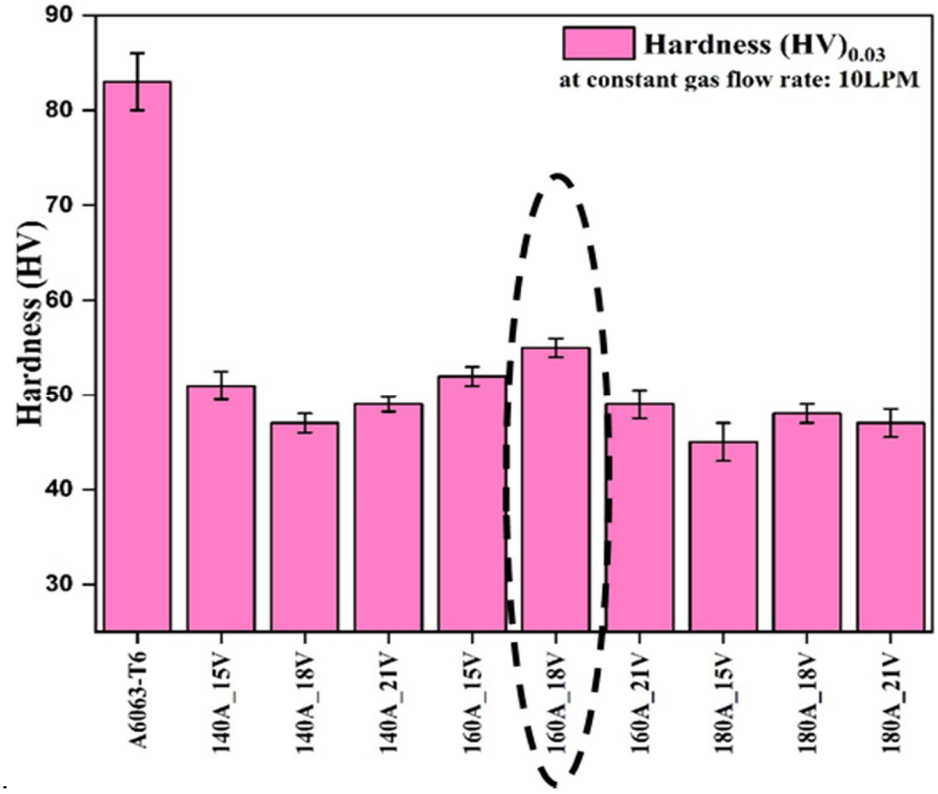

Figure 4.48: Microhardness distribution of A6063 for Fusion zones at gas flow rate of 10LPM

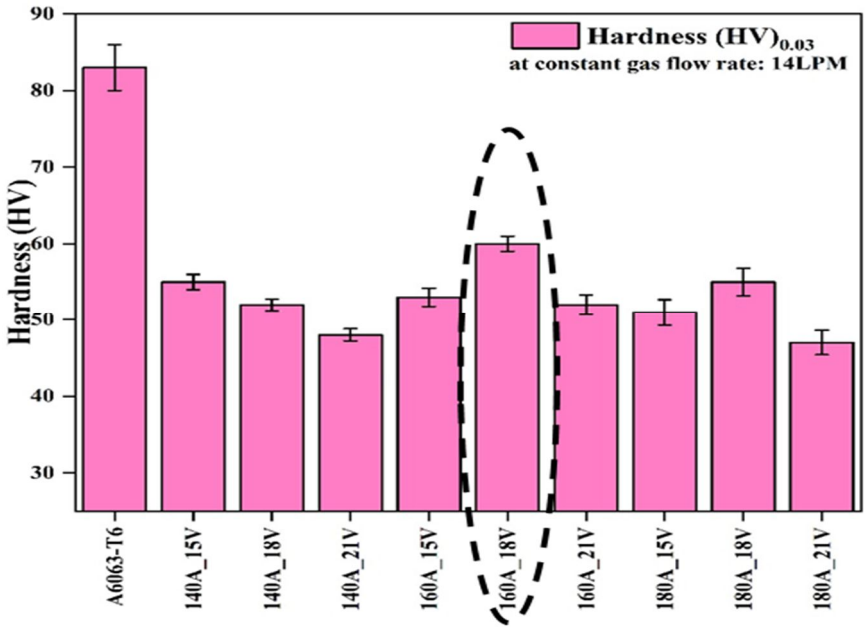

Figure 4.49: Microhardness distribution of A6063 for Fusion zones at gas flow rate of 14LPM

The higher value of hardness in the fusion zone due to the rapid cooling, influenced by increasing gas flow rate. Significantly hardened the welded joints in all zones and increase hardness value by 19.64%. The average hardness and variation in mean hardness

along the transverse direction of fusion zone of A6063 aluminum alloy at 160 amp, 18 volts, and 14 LPM and mean hardness of the MIG welded A6063 aluminum alloy having different current and voltage values at a constant gas flow rate (a) 10LPM.

Variation in mean hardness along the transverse direction of fusion zone of A6063 aluminum alloy at 160 amp, 18 volts, and 14 LPM and mean hardness of the MIG welded A6063 aluminum alloy having different current and voltage values at a constant gas flow rate (b)14LPM

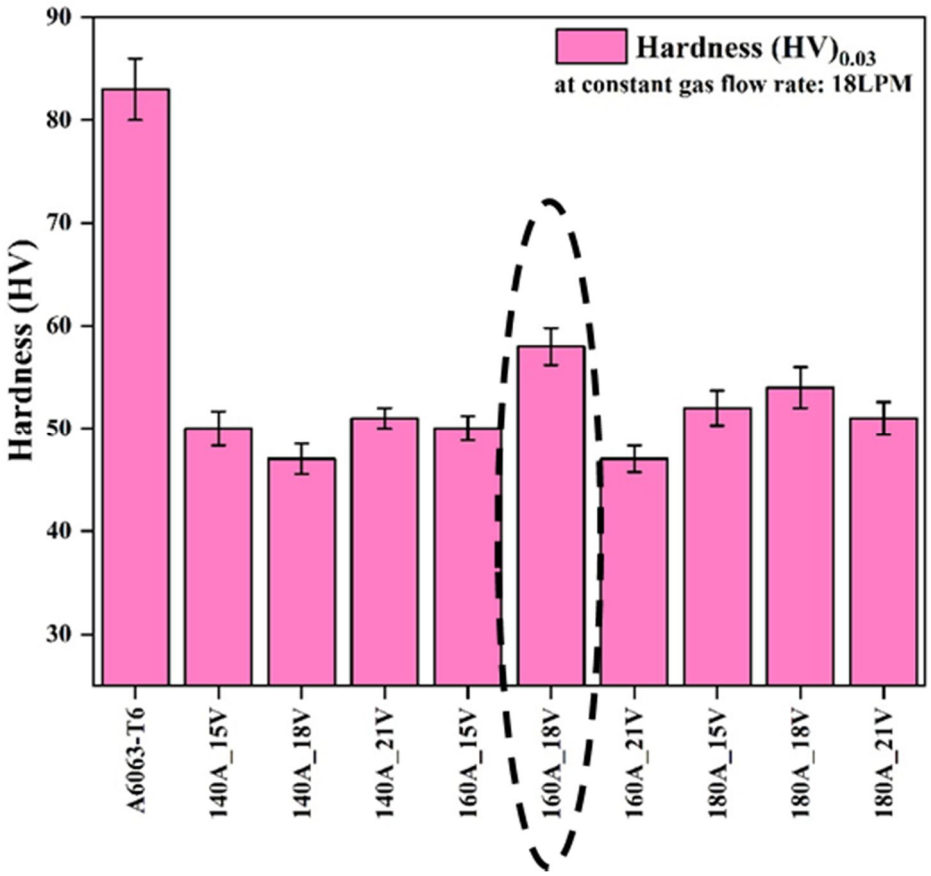

Figure 4.50: Microhardness distribution of A6063 for Fusion zones at gas flow rate of 18LPM

4.8 Effect of Welding Parameters on Tensile Strength

It is inferred from the tensile studies that the fracture occurred at the weld zone of joints made by different welding parameters in all the trials. Tensile test trials showed that there are no many variations in the tensile strength of the weldments.

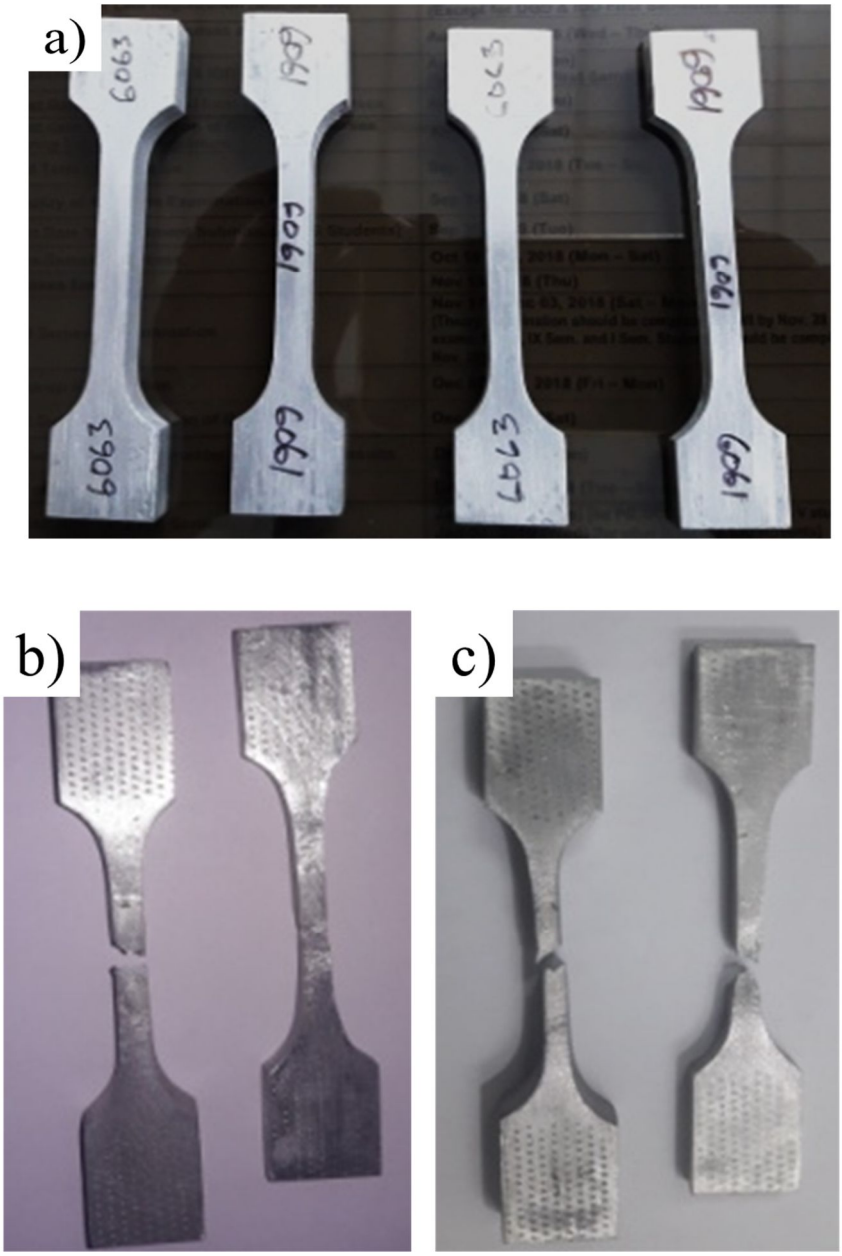

Figure 4.51: Tensile samples of MIG Joints a) Before testing, b) A6061 After testing and c) A6063 After testing

The fractured tensile samples are shown in Fig. 4.50. The experimentally evaluated transverse tensile properties of welded joints obtained by three different kinds of parameters 14lpm,160A,18v (Ar) are shown in Fig. 4.3 and all the data are the average of two measured values. As can be seen, the base case of constant argon produced a weld strength of approximately 220. MPa, while using a gas flow rate 10LPM and 18LPM produced a strength of approximately 215 MPa and 216 MPa produced welds with the strength of 220MPa. Compared to the welded joint made with gas flow rate, the tensile strength of the welded joint made with increased by 5 and 4 MPa respectively.

The tensile testing results suggest that all the fractures occur at the weld zone, consistent with the hardness testing results. It has been shown that the heat input influences the tensile strength of the weld, with an increased heat input resulting in increased strength. The tensile strength of the weld is shown to follow the same trend as the percentage porosity, in that an increasing frequency of alternation produced less porosity and consequently increased the tensile strength of the weld (Campbell et al. 2012).

4.8.1 Tensile Test of A6061 at Different Conditions

The uniaxial tensile test was performed for A6061 aluminium alloy and welded A6061 aluminium alloy were analyzed for Yield strength, Ultimate tensile strength and Percentage elongation has been shown through the bar charts as shown in Fig. 4.51 to Fig. 4.53. Welded joints which were observed from micrograph in earlier section have been analyzed through tensile test results. The maximum strength shown by tensile test was sample with current 160Amp at 18V with gas flow rate of 14LPM. The test properties including yield strength (YS) and ultimate tensile strength (UTS) simultaneously improved with an increase in heat input up to certain limit.

The various strengthening mechanisms in A6061 aluminum alloy which may contribute to increase in strength are as following:

- **Solute strengthening**

Solid solution strengthening is a type of alloying that can be used to improve the strength of a pure metal. The technique works by adding atoms of one element (the alloying element) to the crystalline lattice of another element (the base metal), forming a solid solution. The local non uniformity in the lattice due to the alloying element makes plastic deformation more difficult by impeding dislocation motion through stress fields. In contrast, alloying beyond the solubility limit can form a second phase, leading to strengthening via other mechanisms (e.g. the precipitation of intermetallic compounds).

- **Precipitate hardening**

Precipitation hardening, also called age hardening or particle hardening, is a heat treatment technique used to increase the yield strength of malleable materials, including most structural alloys of aluminium, magnesium, nickel, titanium, and some steels and stainless steels. In superalloys, it is known to cause yield strength anomaly providing excellent high-temperature strength. Precipitation hardening relies on changes in solid solubility with temperature to produce fine particles of an impurity phase, which impede the movement of dislocations, or defects in a crystal's lattice. Since dislocations are often the dominant carriers of plasticity, this serves to harden the material. The impurities play the same role as the particle substances in particle-reinforced composite materials. Just as the formation of ice in air can produce clouds, snow, or hail, depending upon the thermal history of a given portion of the atmosphere, precipitation in solids can produce many different sizes of particles, which have radically different properties. Unlike ordinary tempering, alloys must be kept at elevated temperature for hours to allow precipitation to

take place. This time delay is called "aging". Solution treatment and aging is sometimes abbreviated "STA" in specifications and certificates for metals.

- **Strain hardening**

Strain hardening (also called work-hardening or cold-working) is the process of making a metal harder and stronger through plastic deformation. In the plastic region, the true stress increases continuously i.e. when a metal is strained beyond the yield point, more and more stress is required to produce additional plastic deformation and the metal seems to have become stronger and more difficult to deform. This implies that the metal is becoming stronger as the strain increases. Hence, it is called "Strain Hardening".

At 160A_18V higher strength were observed besides that the values are less due to larger grain size formation in the FZ mainly attribute to the lower cooling rate.

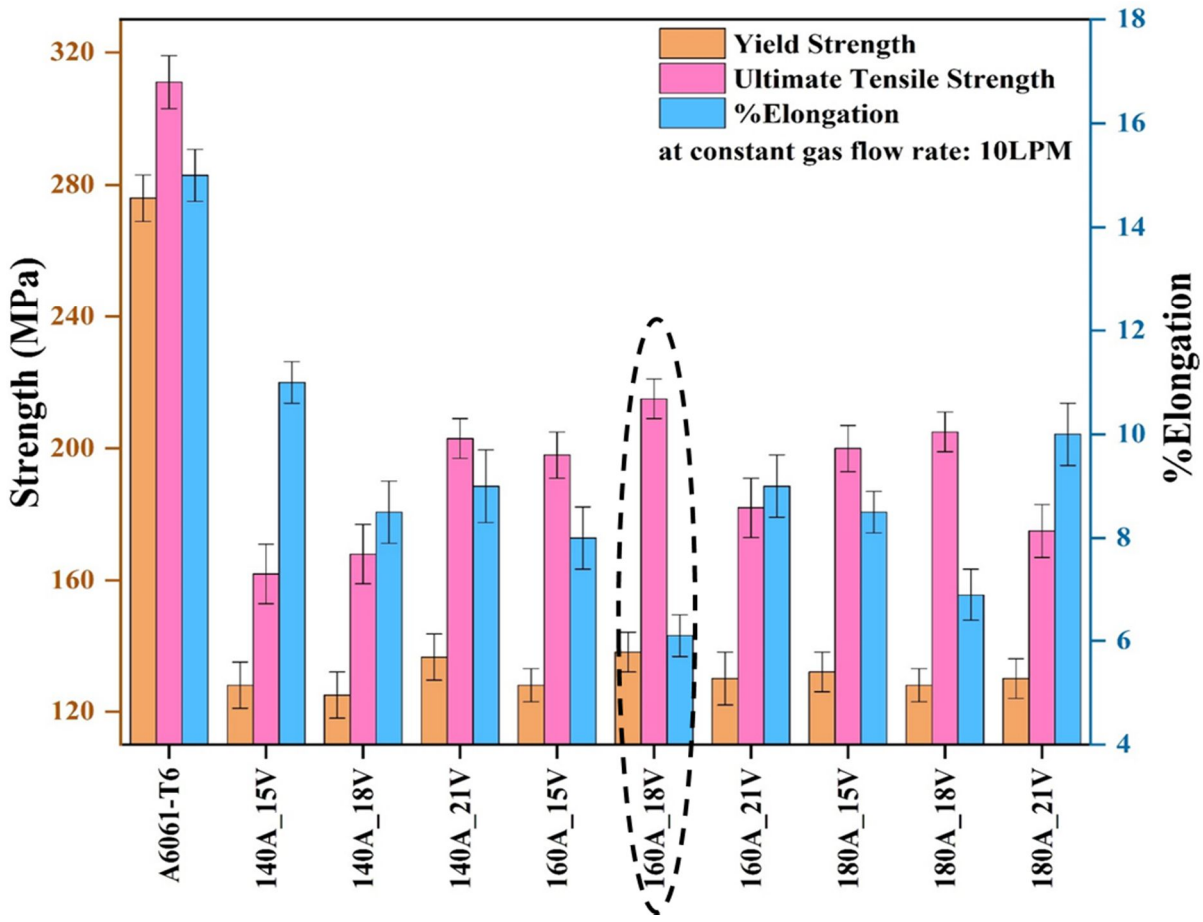

Figure 4.52: The variations in Yield Strength, Ultimate Tensile Strength and %Elongation of A6061 aluminium alloy and welded A6061 at 10 LPM gas flow rate

The uniaxial tensile test was performed for A6061 aluminmum alloy and welded A6061 aluminum alloy there are various strengthening mechanisms in A6061 aluminum alloy i.e Solute strengthening Precipitate hardening Strain rate hardening the test properties including yield strength (YS) and ultimate tensile strength (UTS) simultaneously improved with an increase in heat input up to the certain limit. At 160A_18V higher strength was observed besides that the values are less due to larger grain size formation in the FZ mainly attribute to the lower cooling rate. Which we observed from the micrograph in the fusion zone.

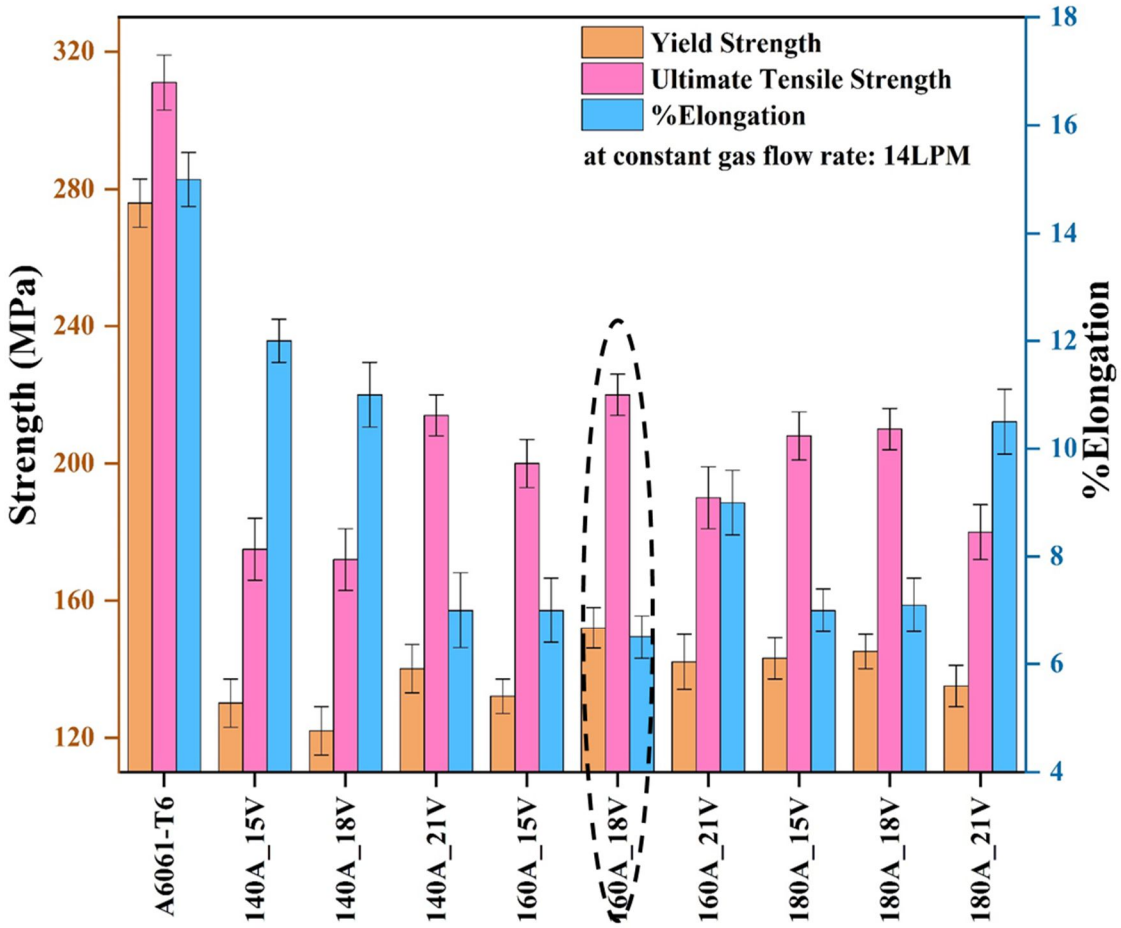

Figure 4.53: The variations in Yield Strength, Ultimate Tensile Strength and %Elongation of A6061 aluminium alloy and welded A6061 at 14 LPM gas flow rate

In this research, welding was carried out with specific parameters so that the welds had a lower amount of porosity. Not only grain size but also porosity, second-phase particle, and precipitated phase can affect the strength of the joints. Porosity in A6061 aluminum alloy weldments by MIG welding deteriorates its mechanical performance. Variations of the strengths based upon the weld specimen's grains size attributed to the Hall-Patch strengthening mechanism.

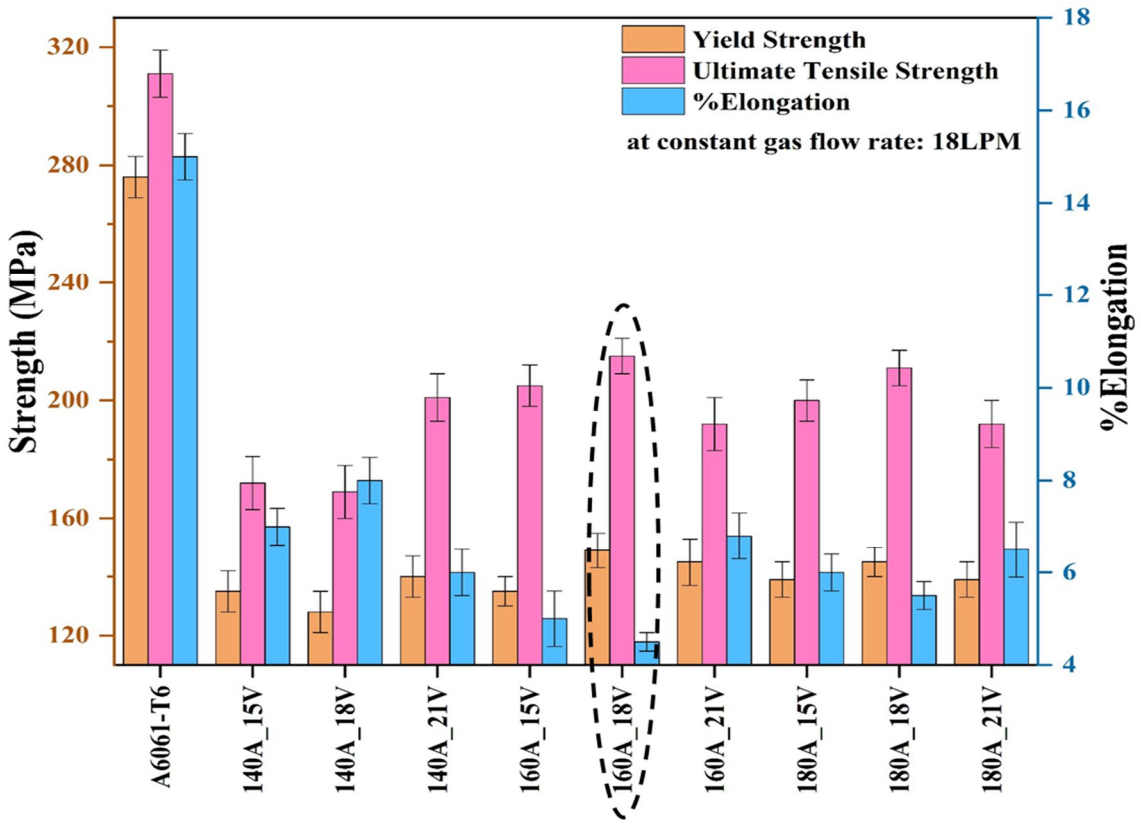

Figure 4.54: The variations in Yield Strength, Ultimate Tensile Strength, and %Elongation of A6061 aluminium alloy and welded A6061 at 18 LPM gas flow rate

Similar variation were observed in case of 18LPM gas flow rate. From the previous tensile data the higher strength were observed at 160A current, 18V volts and 14LPM gas flow rate due to:

- Lack of porosity in weld bead
- Uniform dispersion of precipitates
- Finer grain size in the fusion zone

4.8.2 Tensile Test of A6063 at Different Conditions

The uniaxial tensile test was performed for A6063 aluminium alloy and welded A6063 aluminium alloy were analyzed for Yield strength, Ultimate tensile strength and Percentage elongation has been shown through the bar charts as shown in Fig. 4.54 to Fig.

4.57. Similar strength pattern has been observed for A6063 material under tensile test but quite lower than the A6061 welded joints. The maximum strength shown by tensile test was sample with current 160Amp at 18V with gas flow rate of 14LPM. The test properties including yield strength (YS) and ultimate tensile strength (UTS) simultaneously improved with an increase in heat input up to certain limit.

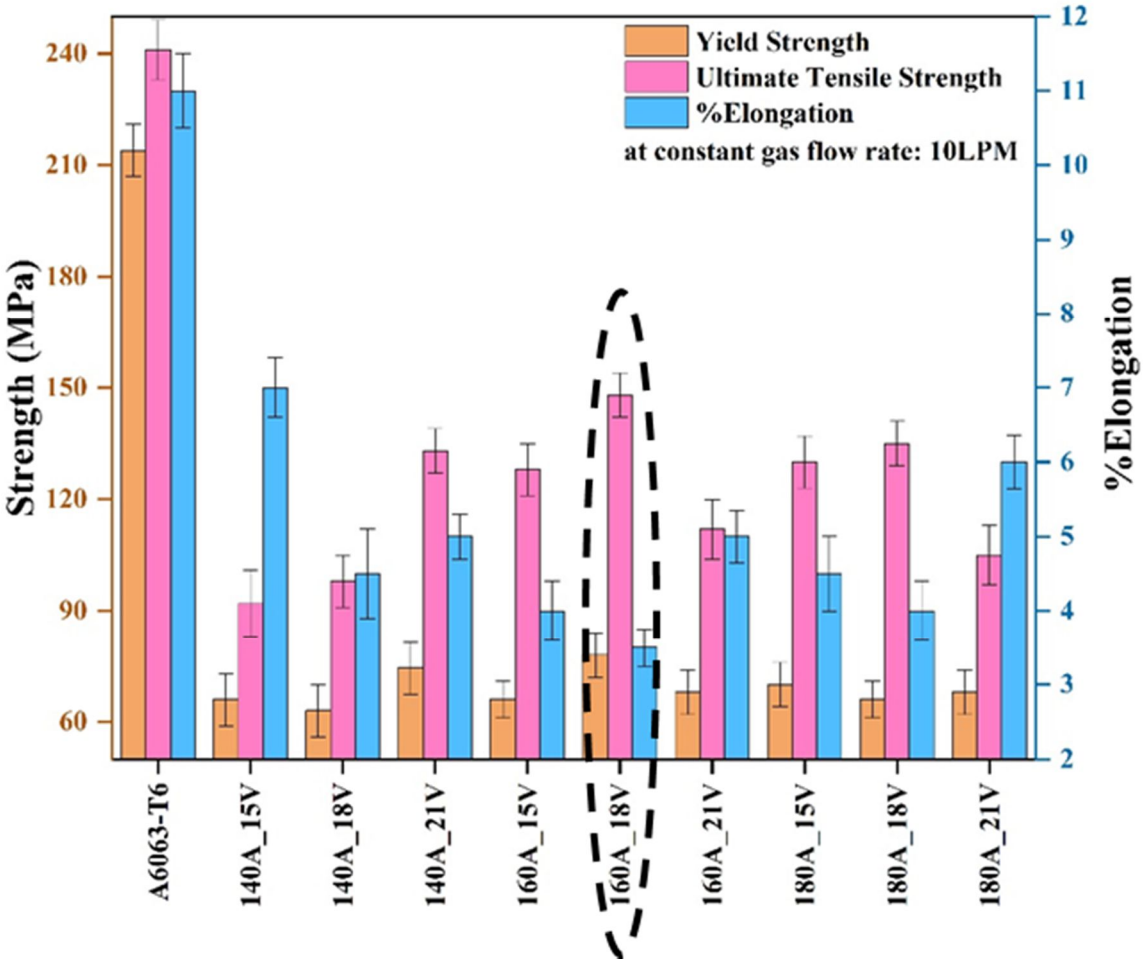

Figure 4.55: The variations in Yield Strength, Ultimate Tensile Strength, and %Elongation of A6063 aluminium alloy and welded A6063 at different working conditions (a) at 10LPM

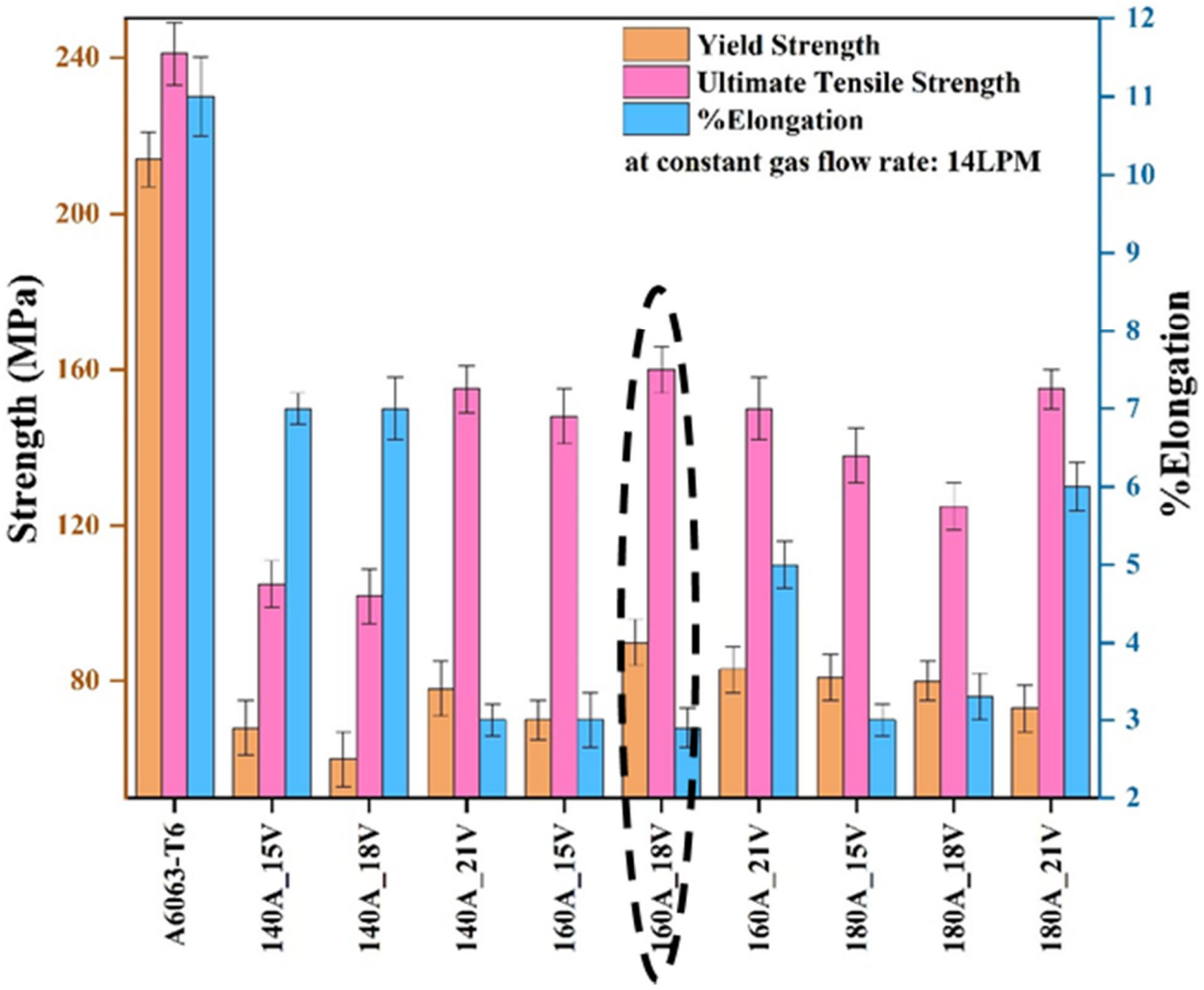

Figure 4.56: The variations in Yield Strength, Ultimate Tensile Strength, and %Elongation of A6063 aluminium alloy and welded A6063 at different working conditions at (b) 14LPM

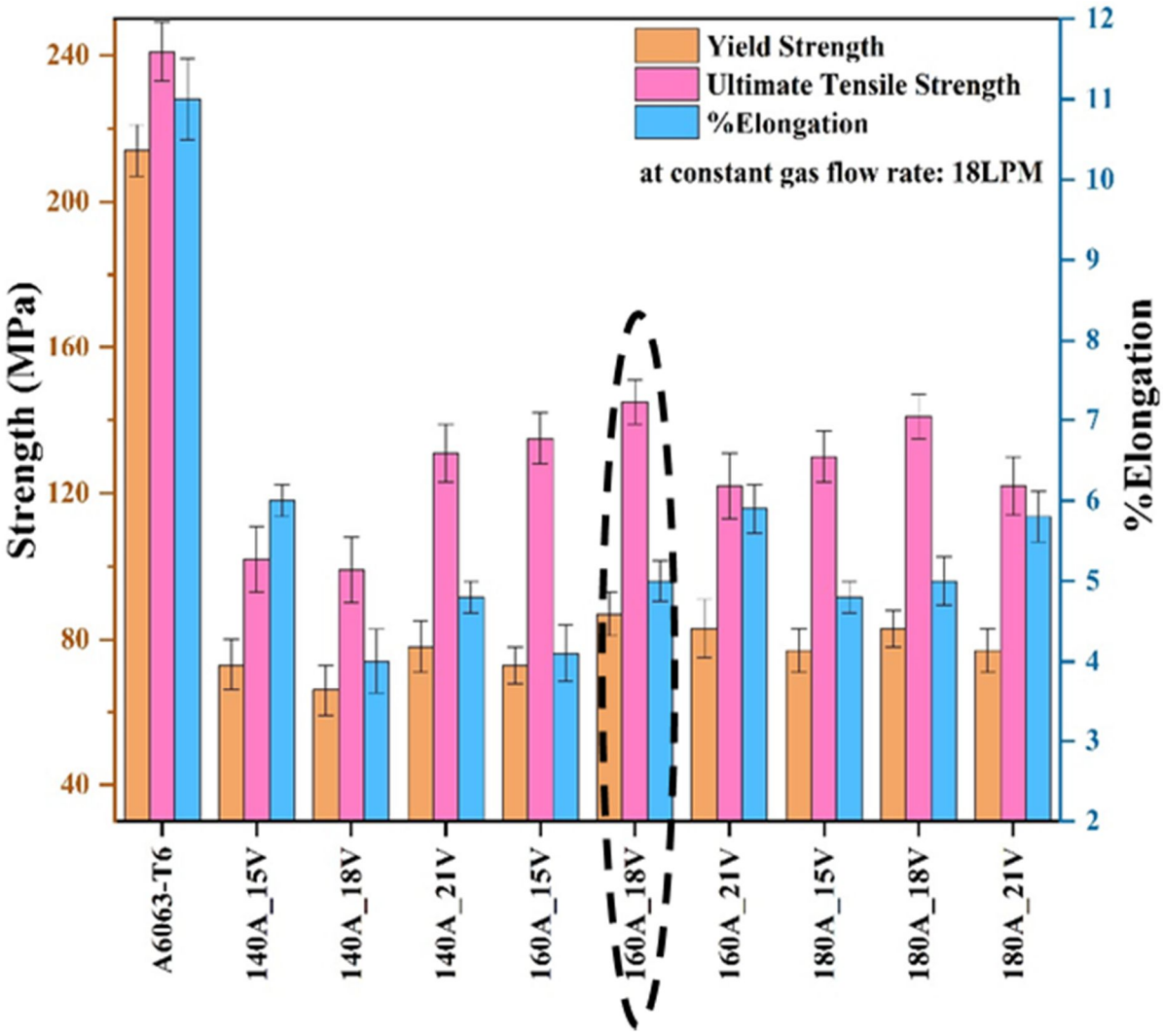

Figure 4.57: The variations in Yield Strength, Ultimate Tensile Strength, and %Elongation of A6063 aluminium alloy and welded A6063 at different working conditions (c) at 18LPM

4.9 Effect of Welding Parameters on Fracture Morphology

The fracture behavior of joints is investigated by scanning electron microscopy (SEM) of a fractured surface of tensile specimens. The fractographs of tensile tested specimens are displayed in Fig. 4.2. It shows the dimples-dominated fracture surfaces. As compared to the parent metal, fracture surface of joint made by pure argon as shielding gas reveals elongated dimples and a pattern indicating failure via ductile fracture

mechanisms. The dimples on the fracture surfaces of joints made using 14LPM gas flow rates were larger than joints made using 10LPM,18LPM gas flow rates. These fine dimples may have originated from the presence of numerous fine precipitates and may also be related to the better dispersion of precipitates. Notably, the entire dimples exhibit an approximate equiaxed pattern on joints made using 14LPM gas flow rate exhibits relatively fine dimples which indicate a ductile type failure. By contrast, a cleavage type fracture mode was observed in the specimen welded by 10LPM and 18LPM gas flow rates due presence of coarse and shallow dimples in the fracture surface. The coarse and elongated dimples result in the reduction of tensile strength.

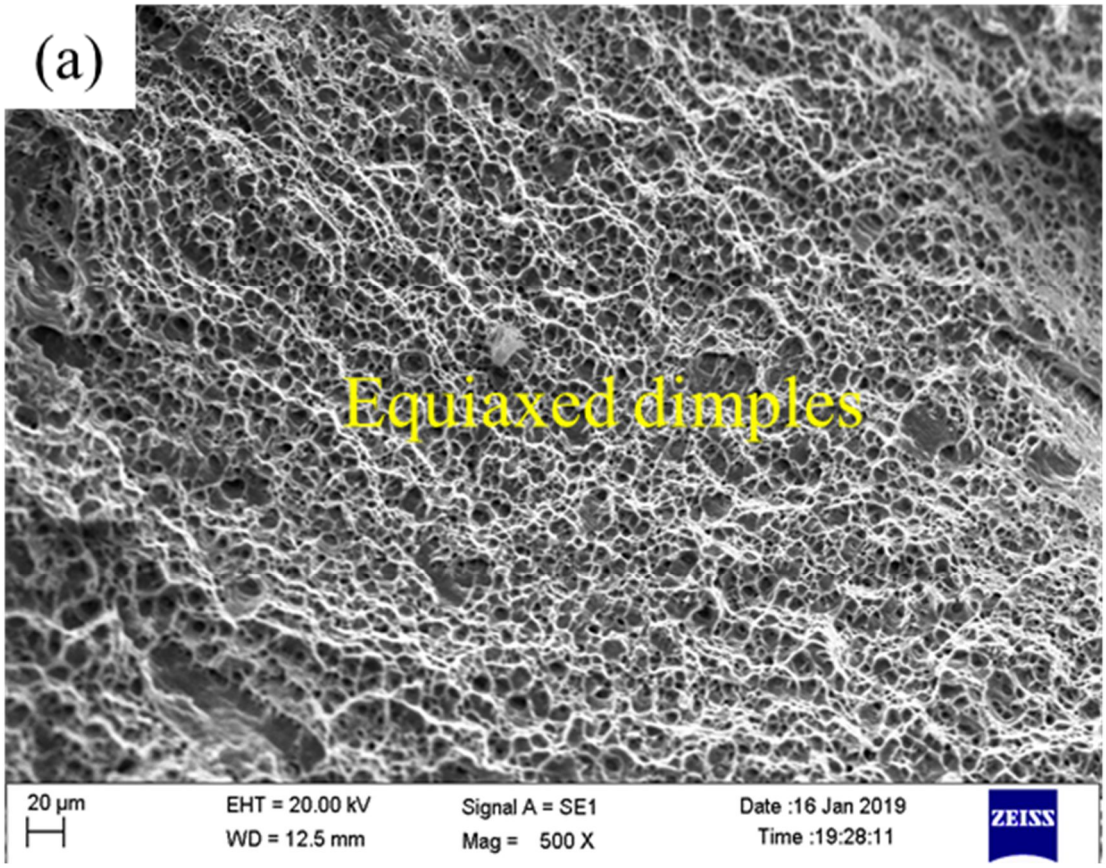

Figure 4.58: SEM micrographs of the fracture surface A6061-T6 equiaxed dimples

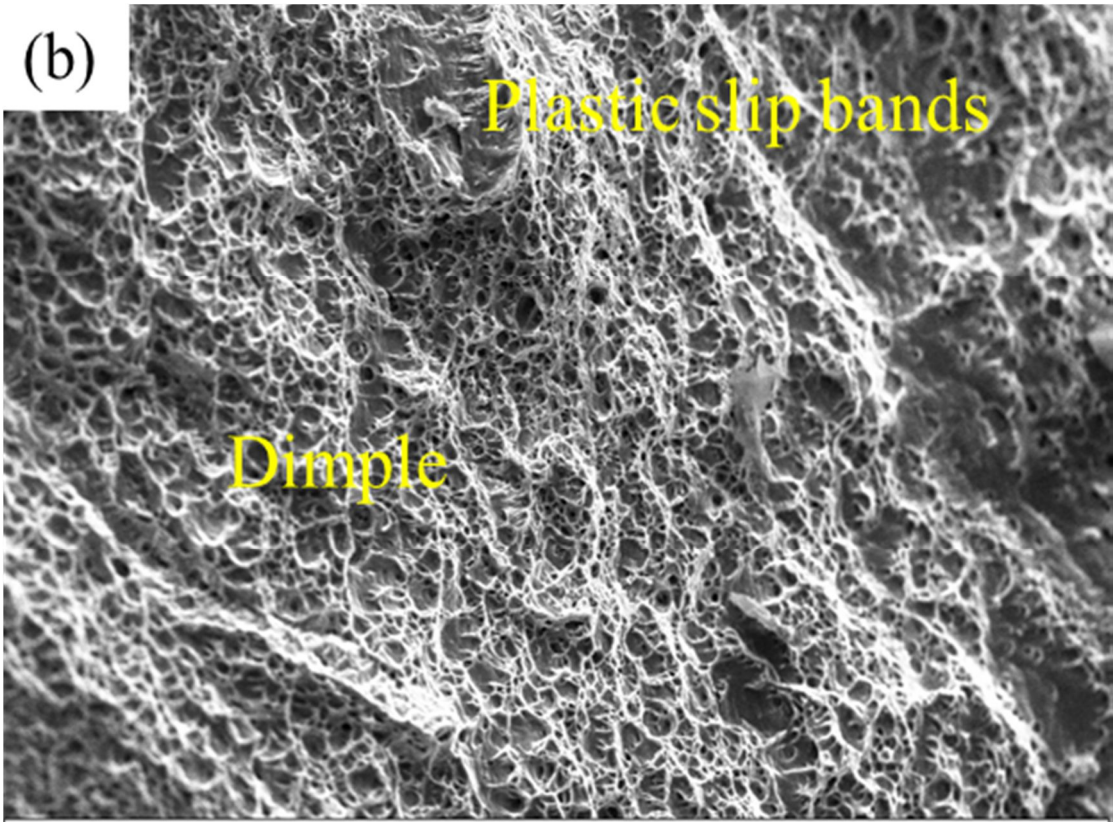

Figure 4.59: SEM micrographs of the fracture surface A6063 T-6 Plastic slip bands Dimple

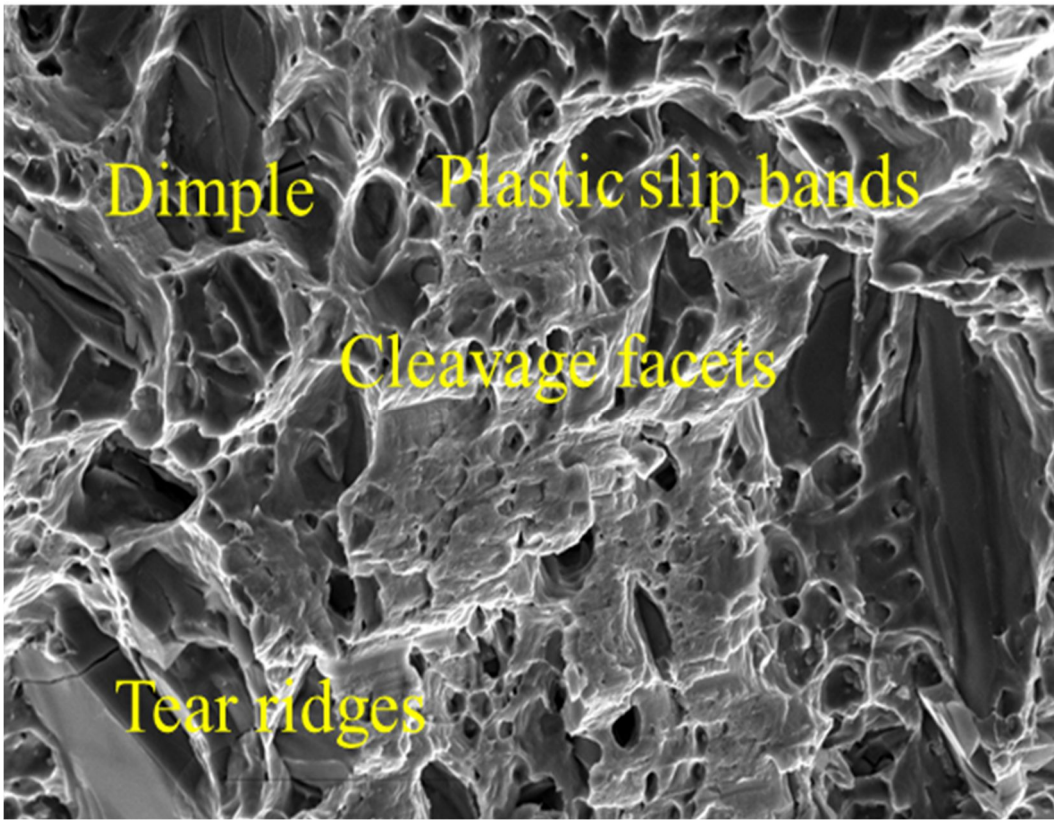

Figure 4.60: SEM micrographs of the fracture surface Welded A A6061 Dimple Plastic slip bands Cleavage facets Tear ridges

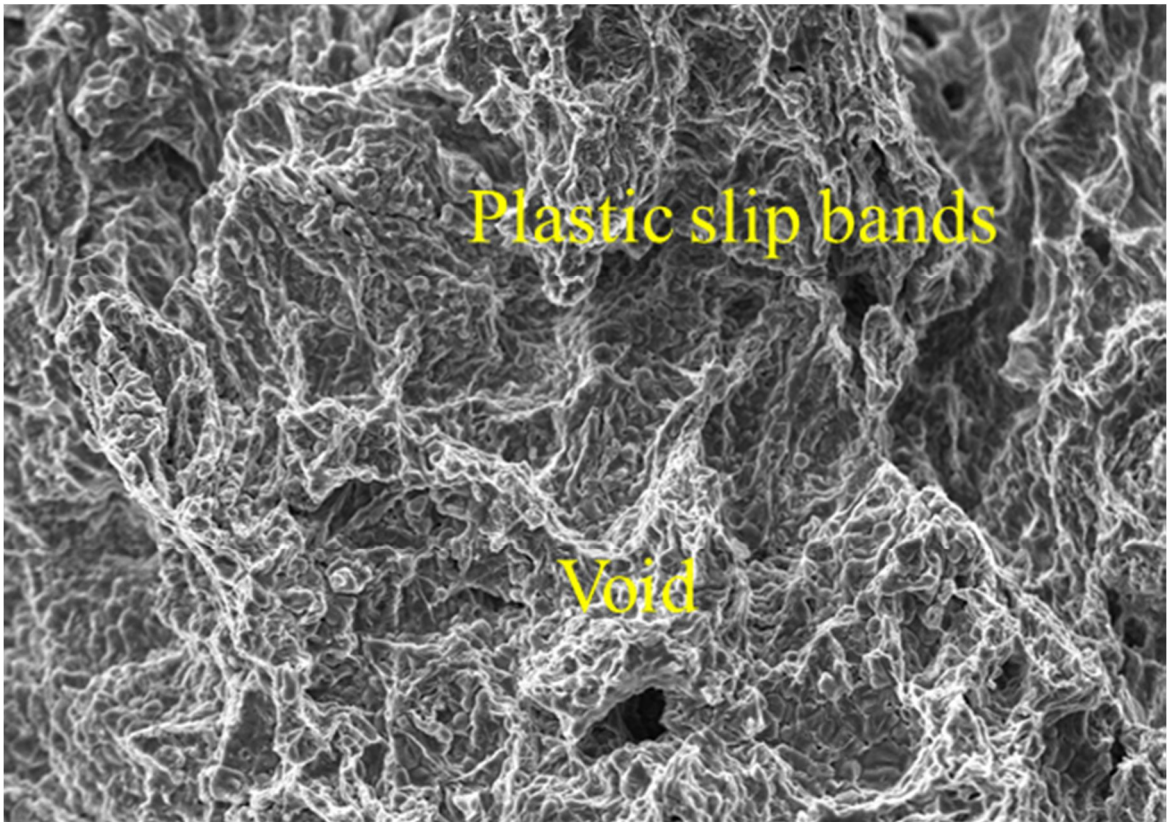

Figure 4.61: SEM micrographs of the fracture surface Welded A6063 Plastic slip bands

From Fig.4.60: SEM micrographs of the fracture surface of Welded A6063shows white plastic slip bands and voids. SEM micrographs of A6061 and A6063 aluminium alloy are consist of a ductile feature. The fracture macrographs revealed that weld metal is the weakest part of the joint. The fracture surface of welded A6061 and A6063 have mixed modes of fracture features. The variation of the pressure in the arc column, caused by differences in the density and ionization potential of 14LPM gas flow rate and 10LPM, 18LPM gas flow rates, results in the periodic impact effect on the weld pool leading to the formation of the metal of the welded joints with a fine-grained structure, high plasticity and strength of the metal (Tazetdinov et al. 2013).

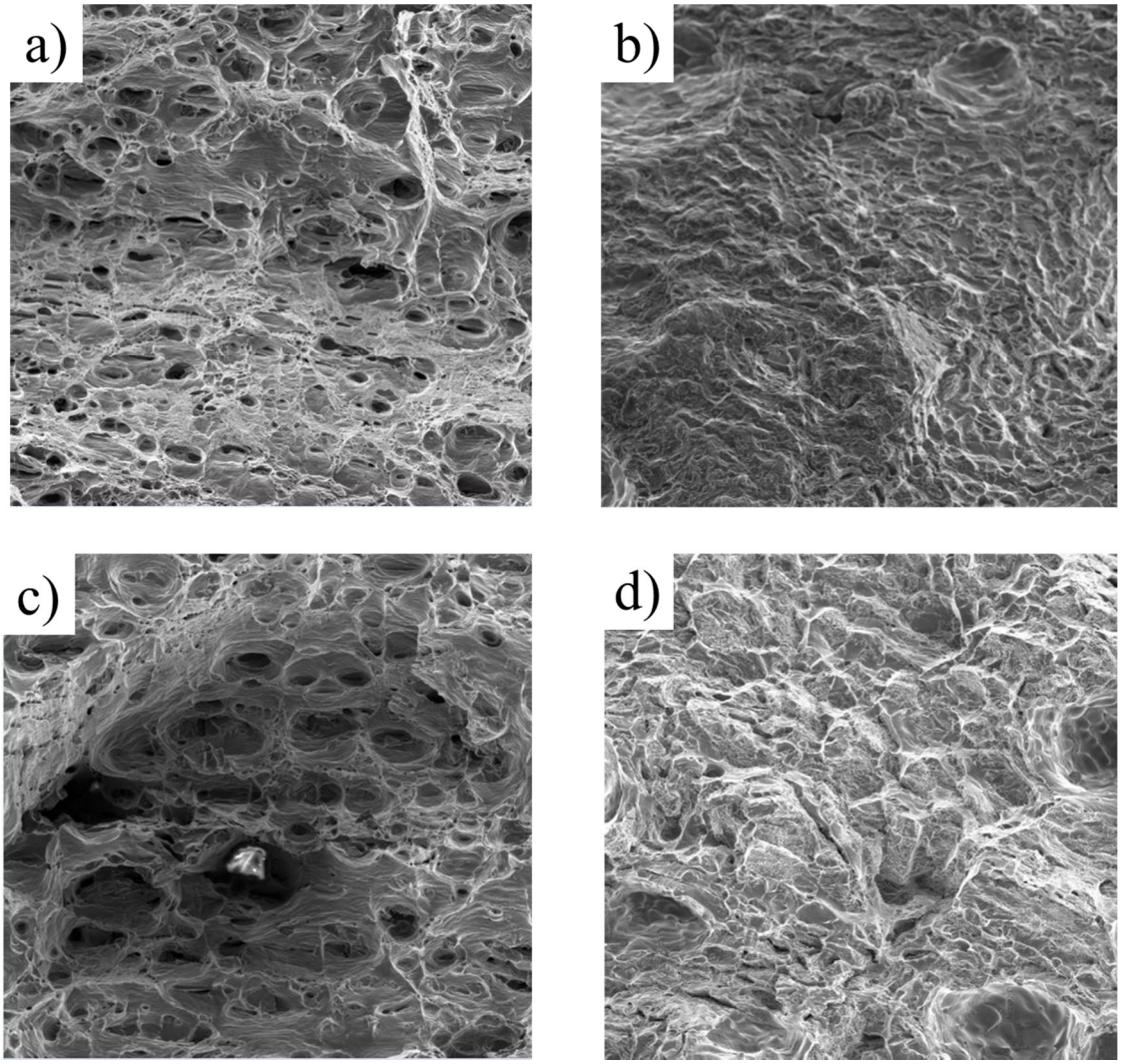

Figure 4.62: SEM images of fracture surfaces of A6061 (a) Base metal (b) 14LPM (c) 10LPM (d) 18LPM

The fractographs of tensile tested joints subjected to post-weld heat treatment are displayed in Fig. 4.62 (a-d). Many cleavages like facets are observed on the fracture surfaces of all gas flow rate samples. The mode of fracture in the joint made using 10LPM, 18LPM is brittle and agrees with the low elongation of the joint 3.5% and 5% respectively.

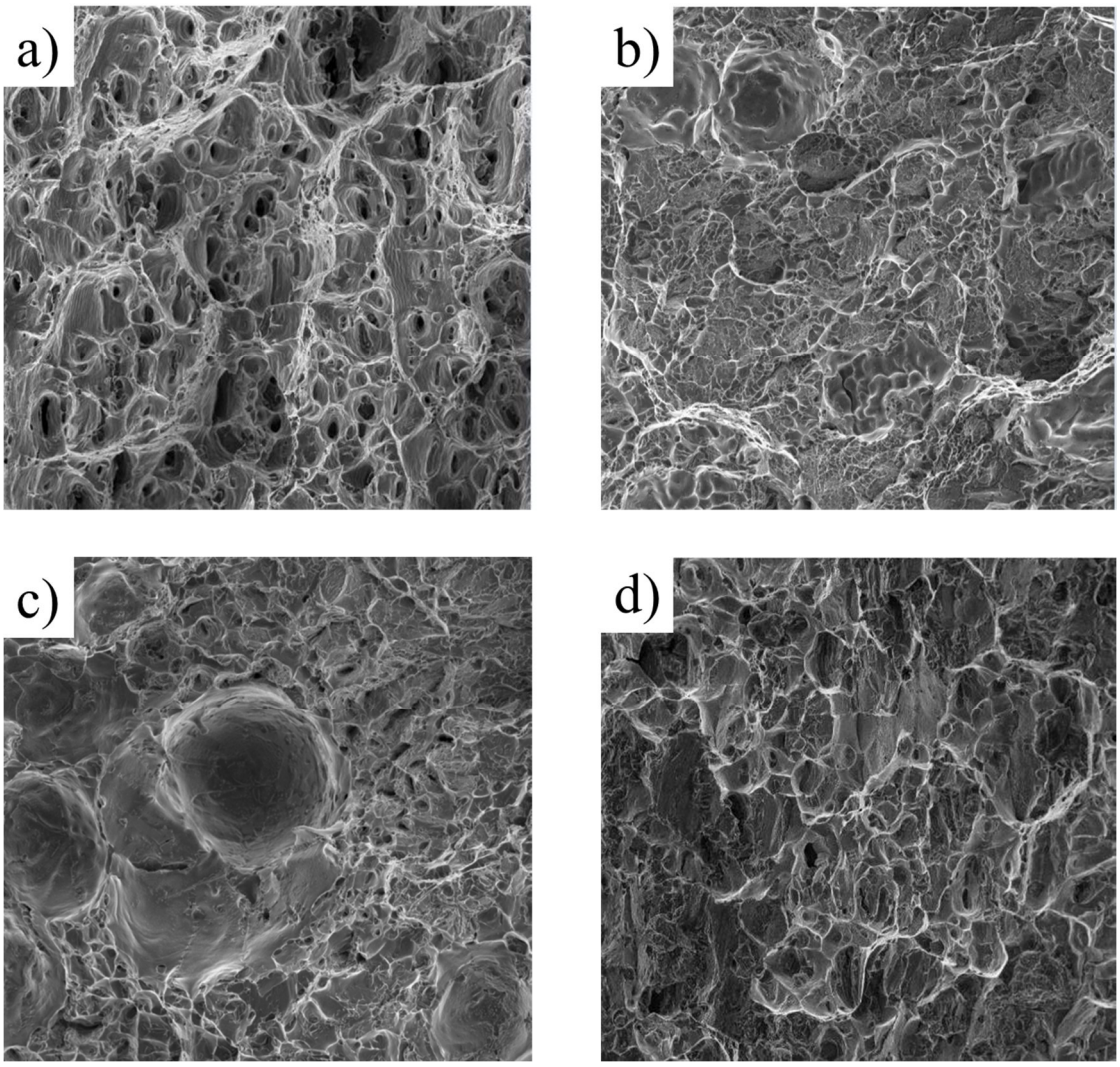

Figure 4.63: SEM images of fracture surfaces of A6063 (a) Base metal, b) 10lpm, c)14 LPM and d) 18lpm)

In addition to cleavage lamellas, various sizes of dimples in the fracture surfaces are observed in the joint made using 14LPM gas flow rate from Fig. 4.62(c) we can see that dimples are distributed in local fractures, at the tips of sharp cracks, inside the tearing fractures. The presence of dimples represents a typical characteristic of ductile cracks, indicating that the ductility is enhanced (Liwei et al. 2012). These observations are in agreement with the high elongation efficiency of the joint.

4.10 Comparison of Welded A6061 and A6063 joints

A comparison of various properties with respect to base material properties has been presenting. Table 4.3 and Table 4.4 shows the base material properties and welded joint properties for different welding variables. The achieved Yield Strength (YS) and Ultimate Tensile Strength (UTS) was 152MPa and 220MPa at 160amp, 18 volts and 14LPM has highest value among all the selected parameters for A6061 aluminium alloy due to heat input providing sufficient heat of fusion and allowing removal of porosity and other defects.

Table 4. 3: Base material A6061 properties

	Hardness (HV)	Yield Strength (MPa)	Ultimate Tensile Strength (MPa)	%age Elongation
A6061	105±3	276±7.5	311±7	15±0.6

Table 4. 4: Comparison table for Welded A6061 aluminium alloy

Gas Flow Rate (LPM)	Current (Amp)	Voltage (Volts)	Welding Speed (mm/sec)	Heat Input (KJ/cm	Hardness (HV)	Yield Strength (MPa)	Ultimate Tensile Strength (MPa)	%age Elongation
10	160	15	2.5	9.216	81	138	215	6.1
14	160	18	2.5	9.216	85	152	220	6.5
18	160	21	2.5	9.216	83	149	216	4.5

In a similar way comparison has been carried out and presented in Table 4.6 and Table 4.7 which shows the base material properties and welded joint properties for different welding variables. The achieved Yield Strength (YS) and Ultimate Tensile Strength (UTS) was 90MPa and 160MPa at 160amp, 18 volts and 14LPM has highest value among all the selected parameters for A6063 aluminium alloy due to welding inputs providing sufficient heat of fusion and allowing removal of porosity and other defects.

Table 4. 5: Base material A6063 properties

	Hardness (HV)	Yield Strength (MPa)	Ultimate Tensile Strength (MPa)	%age Elongation
A6063	83±3	214±7	241±8	11±0.5

Table 4. 6: Comparison table for Welded A6063 aluminium alloy

Gas Flow Rate (LPM)	Current (Amp)	Voltage (Volts)	Welding Speed (mm/sec)	Heat Input (kJ/cm)	Hardness (HV)	Yield Strength (MPa)	Ultimate Tensile Strength (MPa)	%age Elongation
10	160	15	2.5	9.216	55	78	148	3.5
14	160	18	2.5	9.216	60	90	160	2.9
18	160	21	2.5	9.216	58	87	145	5.0

4.11 SUMMARY

The effect of different welding conditions on the mechanical properties of joints made using the MIG welding process was analyzed in detail. The influence of welding condition on heat input of welded joints was comparatively studied using X-ray radiography. AA6061 and A6063 Al joint was characterized by optical microscope, scanning electron microscope, and XRD to understand the metallurgical characteristics of the joint interface.